

Article

Establishing a Data Fusion Water Resources Risk Map Based on Aggregating Drinking Water Quality and Human Health Risk Indices

Ata Allah Nadiri ^{1,2,3,4,*} , Zahra Sedghi ¹ , Rahim Barzegar ^{5,6,7}  and Mohammad Reza Nikoo ⁸ 

- ¹ Department of Earth Sciences, Faculty of Natural Sciences, University of Tabriz, Tabriz 5166616471, Iran
- ² Institute of Environment, University of Tabriz, Tabriz 5166616471, Iran
- ³ Traditional Medicine and Hydrotherapy Research Center, Ardabil University of Medical Sciences, Ardabil 8599156189, Iran
- ⁴ Environmental Geology and Environmental Research Center, University of Tabriz, Tabriz 5166616471, Iran
- ⁵ Department of Bioresource Engineering, McGill University, 2111 Lakeshore, Ste Anne de Bellevue, Quebec, QC H9X 3V9, Canada
- ⁶ Department of Geography & Environmental Studies, Wilfrid Laurier University, Waterloo, ON N2L 3G1, Canada
- ⁷ Ecohydrology Research Group, Department of Earth and Environmental Sciences and The Water Institute, University of Waterloo, Waterloo, ON N2L 3G1, Canada
- ⁸ Department of Civil and Architectural Engineering, Sultan Qaboos University, Muscat P.O. Box 50, Oman
- * Correspondence: nadiri@tabrizu.ac.ir

Abstract: The Drinking Water Quality Index (DWQI) and the Human Health Risk Index (HHRI) are two of the most promising tools for assessing the health impact of water quality on humans. Each of these indices has its own ability to determine a specific level of safety for drinking, and their results may vary. This study aims to develop an aggregated index to identify vulnerable areas in relation to safe drinking water and, subsequently, risk areas for human health, particularly non-cancerous diseases, in the Maku–Bazargan–Poldasht area in NW Iran through the use of a data fusion technique. Nitrate (NO_3^-) and fluoride (F^-) are the predominant contaminants that threaten the local population's health. The DWQI revealed that the majority of the study sites had poor to improper quality for drinking water class. Health risk assessments showed an excessive potential for non-carcinogenic health risks because of high NO_3^- and F^- exposure through drinking water. Children are at a higher risk for non-carcinogenic changes than adults, according to the total hazard index (THI; NO_3^- and F^-), suggesting that locals have faced a lifetime risk of non-cancer changes as a consequence of their exposure to these pollutants. Using data fusion techniques can assist in developing a comprehensive water resources risk map for decision-making.

Keywords: human health risk assessment; drinking water quality index; non-carcinogenic; data fusion; water resources risk



Citation: Nadiri, A.A.; Sedghi, Z.; Barzegar, R.; Nikoo, M.R. Establishing a Data Fusion Water Resources Risk Map Based on Aggregating Drinking Water Quality and Human Health Risk Indices. *Water* **2022**, *14*, 3390. <https://doi.org/10.3390/w14213390>

Academic Editor: Bommanna Krishnappan

Received: 8 August 2022

Accepted: 19 October 2022

Published: 26 October 2022

Publisher's Note: MDPI stays neutral with regard to jurisdictional claims in published maps and institutional affiliations.



Copyright: © 2022 by the authors. Licensee MDPI, Basel, Switzerland. This article is an open access article distributed under the terms and conditions of the Creative Commons Attribution (CC BY) license (<https://creativecommons.org/licenses/by/4.0/>).

1. Introduction

The problem of water shortage and health issues associated with drinking water has become widespread worldwide. In the context of water quality, fluoride (F^-) and nitrate (NO_3^-) concentrations are of particular importance because of the significant health impact they have on humans. In most developing countries, including Ghana, parts of eastern and southern Africa, Turkey, and Iran, high F^- and NO_3^- concentrations have been reported in groundwater [1–4]. It is well known that excessive F^- exposure can damage teeth, bones, and, in some cases, the kidneys. As a result of the inadvertent consumption of F^- by children, adverse effects are known to occur when inadequate F^- amounts are consumed [5]. Moreover, the lack of adequate intake of F^- can lead to an increased risk of dental caries in children, especially in cases where the F^- concentration is lower than

0.5 mg/L in drinking water [6]. Similarly, excessive amounts of NO_3^- in drinking water have the potential to negatively affect human health since they reduce the blood's ability to carry oxygen throughout the body [7,8].

Over the past few years, different water quality indices have been utilized for water quality assessments. The Human Health Risk Index (HHRI) and Drinking Water Quality Index (DWQI) are two indicators that have gained popularity as tools for quantifying groundwater quality and assessing the magnitude of health risks posed to populations exposed to toxic chemicals in the groundwater [9]. However, these indices have undergone some changes in recent years. The major change can be attributed to both the method of interpretation and the calculation procedure [10]. Numerous studies have imitated these methods despite their drawbacks, such as their output classification. Most water quality studies are conducted based on classifications without any rationale as to whether they should be used for drinking purposes, and as a consequence, decisions about drinking water can endanger human health. Therefore, an aggregated method that can combine different water quality indices is needed. In this study, we propose a data fusion method for this purpose. Data fusion has been used in several different settings to resolve the disagreement between information. In general, it refers to using parameters or data in combination to improve the quality of analysis, decrease uncertainty, or obtain new information. See and Abraham [11], describe information fusion as a method of combining information that comes from a number of different resources, a practice that is generally used in the electrical engineering field.

The groundwater quality assessment is not just concerned with the level of contamination and the potential risk of exposure but also with determining and quantifying the distribution of contamination sources [12–15]. Statistical methods such as correlation and factor analysis have been frequently employed to address the contamination origin when dealing with multivariate data. Correlation analysis helps us to understand how hydrochemical parameters are related to one another, allowing us to identify their likely origins. The factor analysis method does not necessitate an understanding of the numeral of sources or features of contaminants but instead provides a method for identifying potential hydrogeochemical processes as well as influencing factors (e.g., geogenic and anthropogenic processes).

Asghari Moghaddam and Fijani [16], conducted research in West Azerbaijan, NW Iran, and showed that the F^- contamination of the water is common in the study area because of the presence of basaltic lavas at a significant depth, which affects the Sari Su river with the release of F^- [17]. Besides F^- contamination, there are high levels of NO_3^- in many parts of the West Azerbaijan Province. However, it has not been explored in the Maku–Bazargan–Poldasht area. Therefore, it is necessary to determine the F^- and NO_3^- concentrations in the drinking water resources of Maku–Bazargan–Poldasht, West Azerbaijan province, in order to determine the quality of water and assess human health risks. This study aims to identify areas where high- F^- and NO_3^- waters formed and then calculate the non-carcinogenic disease risk of inhabitants exposed to NO_3^- and F^- through water supplies using the United State Environmental Protection Agency's approach. Previous studies have revealed a number of major gaps, including (1) NO_3^- contamination has not been detected in water in the Maku–Bazargan–Poldasht, (2) water quality indices have not been classified arbitrarily, and (3) data fusion has not been used to develop a comprehensive risk map for water resources. The current study tries to address these gaps using the proposed methodology.

The novelty of this study is the development of classifications for drinking water quality indices and the enhancement of these classifications over conventional methods of classification, as well as the development of a comprehensive risk map based on a fusion of different types of information. The aim of this study is to develop an aggregated index with data fusion techniques by identifying vulnerable areas in the discussion of safe drinking water and consequently risk areas in terms of human health, with special emphasis on non-cancerous diseases, by: (i) investigating the geochemical features of water quality

samples; (ii) identifying the sources of contaminants; (iii) determining the DWQI and the potential cumulative health risks of contaminated water through multiple exposure pathways (e.g., dermal and oral) for both children and adults; (iv) improving DWQI classification for drinking purposes; (v) developing a new data-fusion-based combined system with aims regarding the health of people in the study area; and (vi) providing a comprehensive health risk map (Figure 1).

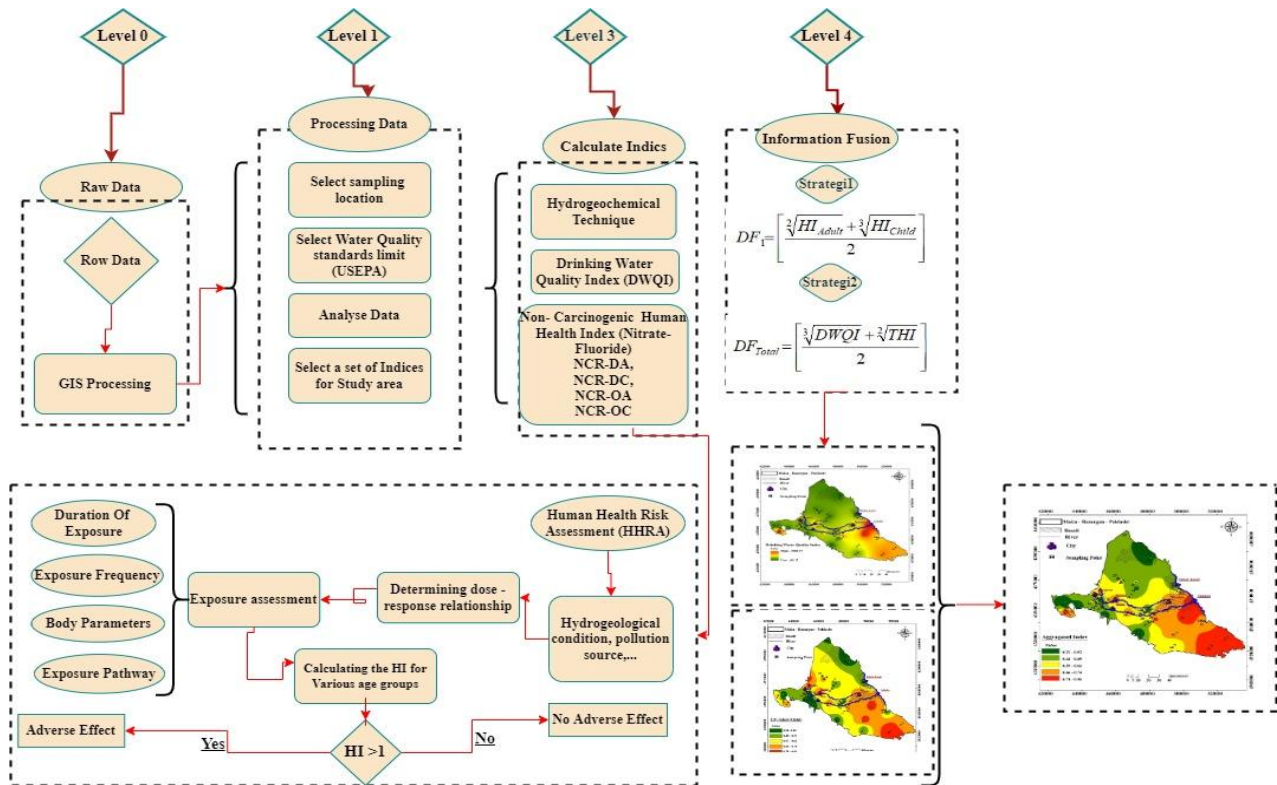


Figure 1. Flowchart of the planned information fusion-based human health risk assessment framework.

A key aspect of this study is the contribution of information about the issue of F^- and NO_3^- contamination in water resources of the study area, as well as valuable evidence that may have a significant impact on the way local authorities manage their risk to reduce the adverse effects of toxic elements on citizens' health. It should be noted that the aspects of the hazard aggregation problem have been discussed at fluctuating points by different authors (e.g., [15,18,19]), but in general, these functions are still in their beginning, especially those that address the last three dimensions. Table 1 lists the selected cases of techniques used in DWQI and HHRI applications.

Table 1. Examples of different techniques used in HHRI and WQI.

Name of Index	Sources	Elements			Methods			Rational Classification (Proposed Classification) for Drinking Water	Application Areas
		Major Ions	Minor Ions	Properties	DWQI	HRA	Fusion Information		
HHRI	[20]	*	*	*		*		Non-carcinogenic health risk assessment of nitrate in bottled drinking water sold	
GIS Base	[21]	*	*	*		*		Calculated HR from NO_3^- in drinking water using the Water Quality Index	
GIS, mathematical base	[22]	*	*	*		*		Assessed hazard index, water resources quality, and hydrochemical analysis using a multivariate method	
GQI/FGQI	[23]	*	*		*			Proposed a new hybrid framework combining GQI with Fuzzy Logic to examine groundwater quality and its spatial variability.	
HHRI	[24]					*		Examined heavy metal contents and evaluated HHRI	
HHRI/WQI	[25]	*	*	*		*		Evaluated based on carcinogenic and non-carcinogenic aspects.	
FHI	[26]	*	*	*		*		Studied trace elements' health risk in drinking water based on the Water Quality Index	
HHRI/EWQI	[27]	*	*	*	*	*		Evaluated the HHRI of F^- concentration in groundwater resources based on fuzzy logic approach	
WQI/HHR	[28]	*	*	*	*	*		Water quality index and human health risk from NO_3^- and fluoride	
Information-Fused Technique	Current study	*	*	*	*	*	*	Water resources contamination; NO_3^- contamination; water quality distribution; health risk	

Note: *: Shows the applied methods.

2. Material and Techniques

2.1. Description of the Maku–Bazargan–Poldasht

The Maku–Bazargan–Poldasht is in West Azerbaijan, Iran, at the Ararat Mountain range's foothills, in the province's north (Figure 2). The Maku–Bazargan–Poldasht is located between longitudes $44^\circ 21'$ and $45^\circ 10'$ and between latitudes $39^\circ 13'$ and $39^\circ 34'$. In the west, it is bordered by Turkey, whereas in the east, it is bordered by the Aras River. The Maku–Bazargan–Poldasht covers nearly 1600 km^2 , of which up to one-fourth is covered with basaltic lavas. This area has three main cities: Maku, Poldasht, and Bazargan. With an average temperature range of -16.2 to $35.1 \text{ }^\circ\text{C}$ and annual mean precipitation of 300 mm , the least and highest precipitation occurred in September and May, respectively. During a typical year, there is approximately 1500 mm of evaporation, three times more than the amount of precipitation expected. The Sari Su and Zangmar rivers are the two main rivers flowing through the study area.

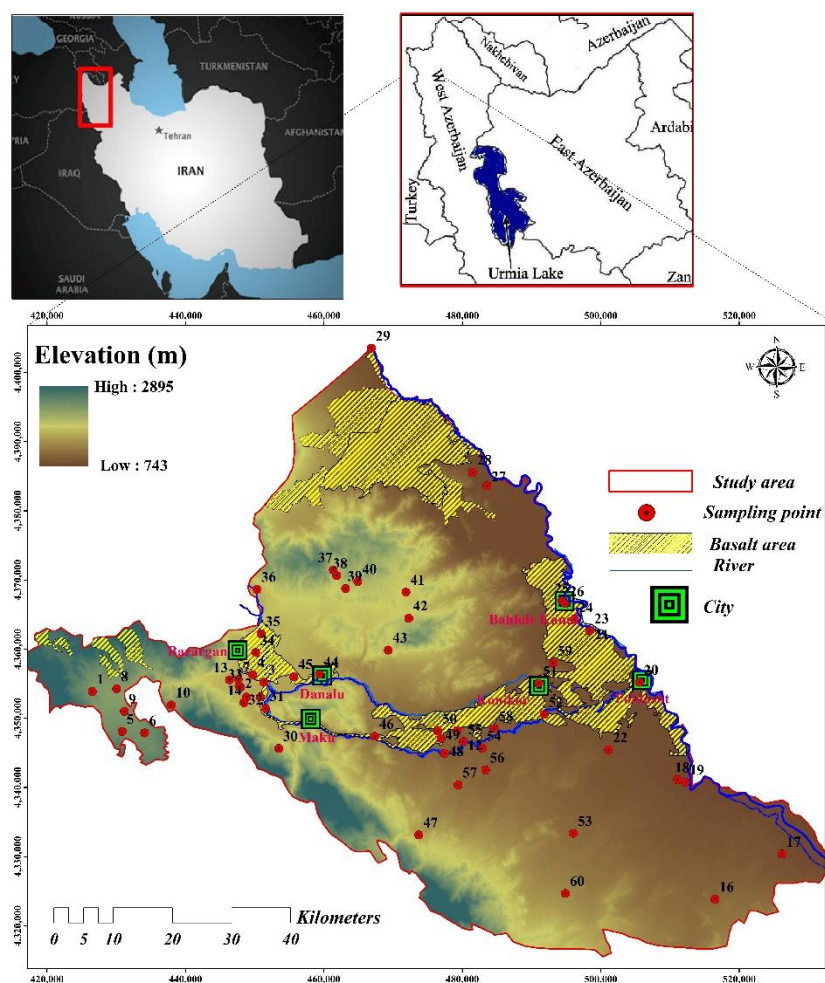


Figure 2. Situation map of the Maku–Bazargan–Poldasht area, drainage system, and sampling locations.

The Maku–Bazargan–Poldasht area is mainly supplied by water resources, which are used for agriculture, drinking, and industry. In addition, 12 large-scale springs and several withdrawal wells discharge groundwater [12]. According to geoelectrical surveying conducted within the Bazargan Plain area, the basalt-alluvium aquifer's thickness is estimated to be about 150 m [12]. Most of the high F^- water resources are found in rock formations formed by basaltic magma (Figure 3). The Maku–Bazargan–Poldasht is predominantly underlain by non-basaltic and basaltic aquifers. Prior reports have indicated a high F^- concentration in the Maku–Bazargan–Poldasht complex aquifers. The presence of F^- in some areas (called the mixing zone) is caused by the mixing of groundwater from basaltic and non-basaltic origins. Phyllite–schist and gneiss, which are the main water-bearing rocks in the region, have small amounts of primary porosity. The secondary porosity of these formations, which is found in the form of fissures or fractures, enables groundwater to be actively transported through the rocky formation, thus acting as a groundwater reservoir. The majority of these zones can be found in basaltic aquifers and some of them can be found in non-basaltic aquifers. As a result of drinking water from basalt springs and wells, residents in the region suffer from dental fluorosis [12].

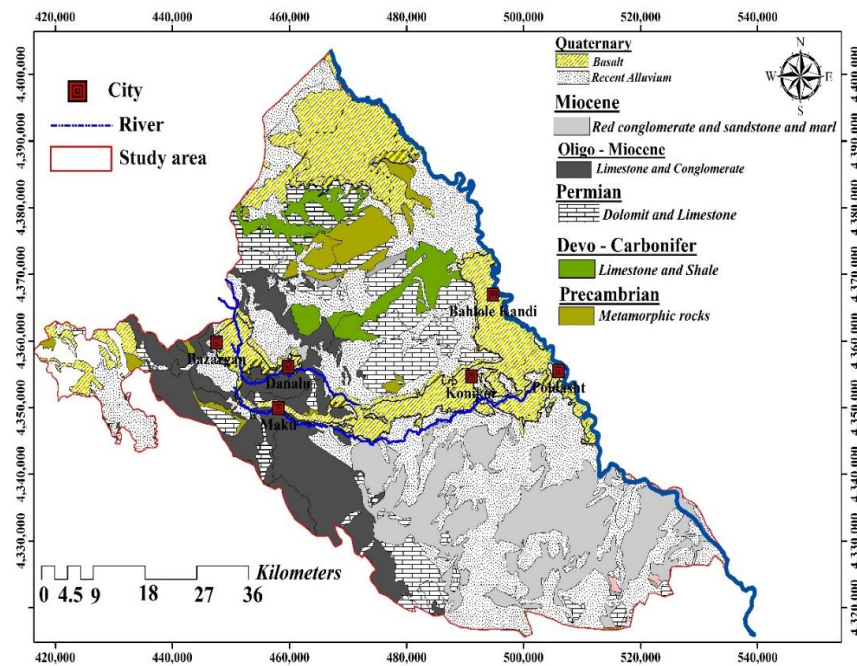


Figure 3. Geological map of the Maku–Bazargan–Poldasht area.

2.2. Water Sampling and Analysis

Sixty samples were gathered from springs, rivers, and wells in January 2021. These resources provide a large volume of water for consumption and irrigation. Electrical conductivity (EC) and pH were measured directly in the field during sample collection. Potassium (K^+) and sodium (Na^+) were measured with a flame photometer. A UV single-beam spectrophotometer (UV-1200, Labman Scientific Instruments Pvt. Ltd, Chennai, India) was used for Sulphate (SO_4^{2-}), NO_3^- , nitrite (NO_2^-), ammonium (NH_4^+), and bromine (Br^-). Bicarbonate (HCO_3^-), carbonate (CO_3^{2-}), chloride (Cl^-), magnesium (Mg^{2+}), and calcium (Ca^{2+}) were analyzed using the titration approaches [29]. The F^- concentration was calculated by utilizing an ion-selective electrode. Chemical analysis was validated using an ion balance. The sum of cations and anions must be equal according to the principle of neutrality. A cation–anion balance error [30], was calculated as follows:

$$CBE\% = \frac{\sum z \cdot m_c - \sum z \cdot m_a}{\sum z \cdot m_c + \sum z \cdot m_a} \times 100 \quad (1)$$

where A and C are the concentrations of $HCO_3^- + Cl^- + SO_4^{2-}$ and $Ca^{2+} + Mg^{2+} + Na^+ + K^+$, respectively, in meq/L. Additionally, charge balance is the ratio of the ionic balance error. The accuracy of ionic measurements was measured through the Charge Balance Error percentage (CBE%). A CBE% within the range of $\pm 5\%$ is accepted as a good analysis measure [31].

2.3. Physicochemical Characteristics of Water Resources

A statistical investigation of the physicochemical parameters of water resources measured in the field and the laboratory are presented in Table 2. There was a major difference between the median and maximum values of Na^+ , Ca^{2+} , Cl^- , SO_4^{2-} , NO_3^- , NO_2^- , and CO_3^{2-} , and the maximum values were more than five times the median values, implying the presence of some external contaminants in the groundwater [32]. The EC value varied between 525 and 5530 $\mu S/cm$, with an average value of 1503 $\mu S/cm$. It was found that 65% of the samples were freshwater, 20% were brackish, and 15% were saline, according to the EC classification for water samples (i.e., fresh: 1500 S/cm; brackish: 1500–3000 S/cm; saline: >3000 S/cm). The pH values of the water samples in the Maku–Bazargan–Poldasht area ranged from 7.37 to 8.3, indicating a slightly acidic to a slightly alkaline environment.

According to the US EPA, all samples fell within acceptable limits regarding the pH parameter. Na^+ concentrations ranged between 16 and 1001 mg/L, with an average value of 221 mg/L. According to EPA standards [33], the maximum allowable concentration of Na^+ for drinking water was 200 mg/L. Table 2 shows that 24 sampling sites exceeded the standard threshold for drinking purposes. In total, 10% of the samples contained Ca^{2+} concentrations that ranged between 32 and 518 mg/L, with a mean concentration of 102 mg/L, which was larger than the acceptable limit (i.e., 100 mg/L). Mg^{2+} and K^+ concentrations varied between 11–245 mg/L and 3–70 mg/L, with 65 and 12 mg/L mean values, respectively. In total, 95% of the samples violated the standard threshold of 30 mg/L. In the Maku–Bazargan–Poldasht area, the Cl^- concentration in the water resources varied from 4 to 769 mg/L with a mean of 132 mg/L. According to the results, about 15% of them exceeded the 250 mg/L drinking water guideline [33]. Additionally, HCO_3^- and CO_3^{2-} concentrations showed a wide range of 107–536.5 mg/L and 0–80.6 mg/L, respectively. On the other hand, there was no recommended value for either one. The SO_4^{2-} content ranged from 5.5 to 9079 mg/L with an average of 1263 mg/L, and the greater part of the samples (80%) were within the acceptable drinking limit of 250 mg/L. In this area, the presence of high levels of SO_4^{2-} may be attributed to little rain and strong evaporation as well as an aquifer medium abundant in sulfate. The concentration of SO_4^{2-} in the water was also affected by the contact between the water and the rock as well as evaporation-induced enrichment. NO_2^- concentrations in the samples ranged from 0 to 4.79 mg/L, with about 95% having NO_2^- concentrations more than the standard limit of 1 mg/L [33]. In summary, the average concentration of major cations was in the order of $\text{Na}^+ > \text{Ca}^{2+} > \text{Mg}^{2+} \gg \text{K}^+$. A correlation analysis was conducted to determine whether there was a consistent relationship between the hydrochemical parameters. It was determined through SPSS that the data were normally distributed to determine which correlation analysis approach (i.e., parametric or nonparametric) should be used in order to determine the most appropriate correlation analysis approach. As a result of the non-normal distribution of the hydrochemical data, Kendall's correlation test, a method of nonparametric correlation analysis, was applied to the hydrochemical data.

Table 2. Statistical analysis of the measured water parameters compared to US EPA standard (2014).

Parameter	Units	Range	Mean	Standard Deviation	US EPA	Type of Problem	Samples Exceeded US EPA Limit
October 2021							
<i>Institute measurements</i>							
EC	$\mu\text{S/cm}$	525–5530	1503.9	1099.27	1000		62%
pH	-	6.7–8.37	7.37	0.37	7.5		28%
<i>Major Elements</i>							
Na^+	mg/L	16–1001	221.39	217.63	200		40%
K^+	mg/L	3–70	12.44	10.15	12		45%
Ca^{2+}	mg/L	32–518	102.70	82.68	200		9%
Mg^{2+}	mg/L	11–245	65.68	51.56	30		81%
Cl^-	mg/L	4–770	132.02	162.25	250		17%
SO_4^{2-}	mg/L	6–9079	479.21	1263.94	250		20%
HCO_3^-	-	107–537	265.59	109.48	300		-
F^-	mg/L	0.39–10	2.94	2.43	1.5	Caused fluorosis	48.33%
Br^-	mg/L	0–1	2.78	4.74	0.1		83.3%
<i>Nutrients</i>							
NO_3^-	mg/L	0.23–169	32.22	39.04	10	Methemoglobinemia	75%
NO_2^-	mg/L	0–5	0.32	0.86	3		4%
NH_4^+	mg/L	0–4	1.05	1.05	0.05		76.6%

2.4. Multivariate Statistic

Pre-processing of the data (i.e., normalization, log transformation) was performed to standardize the measured water quality parameters and remove the impact of their diverse units on the multivariate statistics. Then, the Pearson correlation analysis of the water quality parameters was calculated to decipher the relationship between the parameters. Significance (p value) and strength (r) were essential factors when determining the significance of relationships. The higher the r value, the stronger the relationship, and in this study, $r > 0.7$ was considered to be a strong relationship, while $0.5 < r < 0.7$ and $r < 0.5$ were deemed to be average and weak relationships, respectively. Factor analysis (FA) is usually utilized to determine the hidden dimension, which may not be described by direct analysis. In total, 14 water quality parameters, including pH, EC, Ca^{2+} , Mg^{2+} , Na^+ , K^+ , HCO_3^- , SO_4^{2-} , Cl^- , NO_3^- , F^- , NO_2^- , Br^- , and NH_4^+ , were considered when carrying out the FA. The Kaiser's criterion and varimax rotation technique [34], were used to improve factor loadings, achieve a simple structure, and find factors with eigenvalues greater than 1. Consequently, factor loadings greater than 0.75 were well thought-out as high, whereas factor loadings between 0.50 and 0.75 were considered medium [35]. As mentioned above, NO_3^- contamination was severe in the Maku–Bazargan–Poldasht area. The oxidative conditions of the water resources in the Maku–Bazargan–Poldasht area facilitates the conversion of NO_2^- and NH_4^+ contaminants to NO_3^- as a result of the nitrification process [36]. According to the linear correlation between TDS and $\text{NO}_3^- + \text{Cl}^- / \text{HCO}_3^-$ [37], a positive correlation coefficient of 0.7 was determined (Figure 4), indicating that the water resource under study was contaminated by anthropogenic activities.

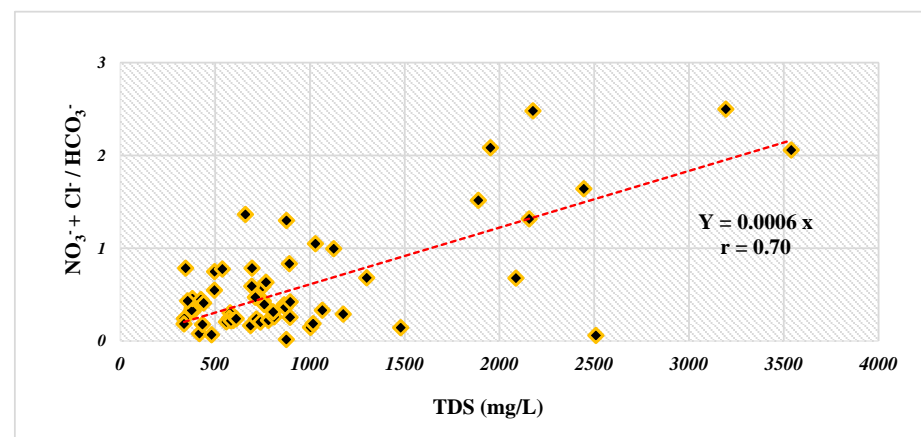


Figure 4. Bivariate plot to check the relation between TDS and $\text{NO}_3^- + \text{Cl}^- / \text{HCO}_3^-$.

The NO_3^- in water resources can result from anthropogenic and geogenic inputs. It is common for water resources to contain nitrogen concentrations below 10 mg/L, and those above this limit are considered anthropogenic. Figure 5 shows that most samples in the Maku–Bazargan–Poldasht area had NO_3^- concentrations exceeding the standards limit of 10 mg/L [33], suggesting that the anthropogenic NO_3^- contamination affected water quality in the study area. Fluorosis is a prevalent disease in tropical climates, but this is not entirely the case. Water with high F^- concentrations in wide geographical belts are related to: (i) sediments with marine sources in the mountainous regions; (ii) igneous rocks; and (iii) gneissic and granitic rocks. A classic example of the first reason covers Iran and Iraq through Turkey and Syria to the Mediterranean region, from Algeria to Morocco [38]. The F^- contamination was as severe as the NO_3^- contamination in the study area. Approximately 50% of the sampling sites revealed F^- and NO_3^- concentrations higher than the recommendations given by [33] (Figure 5). Studies have shown that approximately 90% of F^- in drinking water is absorbed in the digestive system, while only 30–60% of F^- is absorbed in food [33]. Therefore, there is a risk of skeletal fluorosis and dental fluorosis with excessive F^- concentrations, e.g., between 1.5 and 5.0 mg/L. High

levels of F^- in drinking water can cause more diseases, such as hypertension, neurologic disorders, Alzheimer's disease, etc., posing a serious threat to human health [39]. According to studies conducted by the Poldasht Health Center, available data and information confirm the prevalence of bone fluorosis [40].

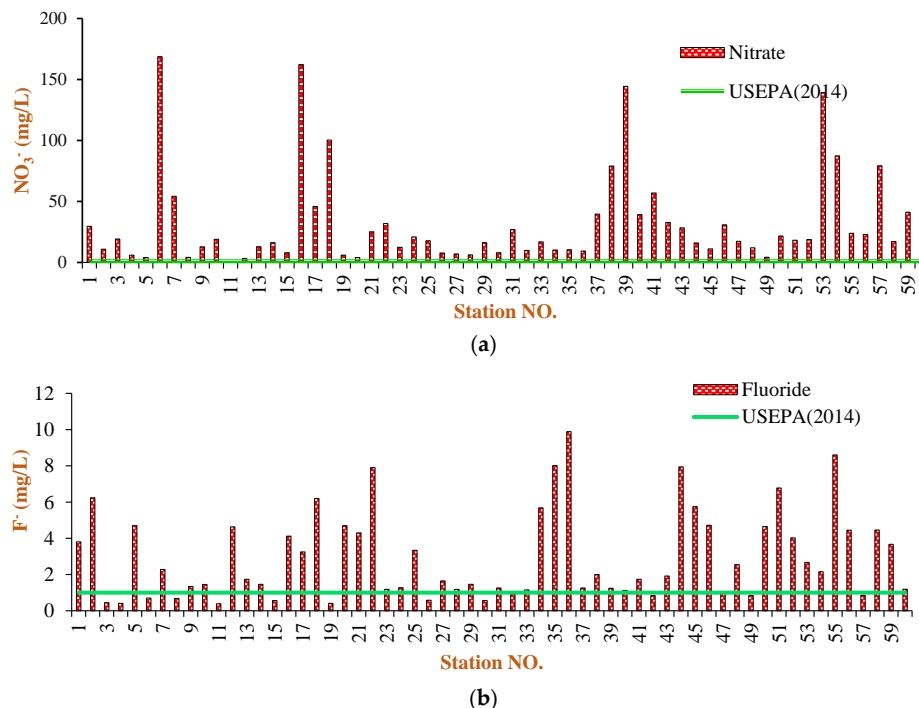


Figure 5. Excessive contaminants (non-carcinogenic) at the sampled water resources ((a): Nitrate; (b): Fluoride) [33].

F^- concentrations are often relative to the level of water–rock contact because F^- mainly originates from geology [41,42]. The study region is primarily occupied by basalts, which contain a large amount of F^- -bearing minerals [43]. The F^- concentration likely increased because of this in the study area. Compared to NO_3^- contamination, F^- contamination was highly severe in the study area. The NO_3^- concentration in the Maku–Bazargan–Poldasht water resources ranged from 0.23 to 167 mg/L with a mean of 32.2 mg/L. The threshold of public health standards on NO_3^- in drinking water set by the US EPA is 10 mg/L. Overall, 75% of the samples had NO_3^- concentrations that exceeded the US EPA standard of 10 mg/L (Table 2). In natural water resources, the higher concentrations of NO_3^- can have anthropogenic origins such as unsuitable surplus disposal, severe agriculture practices, and animal surplus [18,19,43]. Figure 5 shows a bar chart that shows the NO_3^- and F^- values of the study region relative to the US EPA. A wide variation in F^- concentrations are observed (Table 2), varying between 0.39 and 9.89 mg/L, with a mean of 2.94 mg/L. On the other hand, in most samples (54%), the F^- concentration exceeds its maximum allowable threshold (1.5 mg/L) for drinking water [33].

2.5. Drinking Water Quality Index (DWQI)

The Drinking Water Quality Index (DWQI) exposes the general quality of drinking water. This index can be determined by standardizing each hydrogeochemical parameter [44]. The DWQI switches the samples' water quality parameters into a sole code and the analysis of water quality information is compared with data from the World Health Organization to check their appropriateness for drinking in Appendix A (Table A1). The DWQI calculation is based on three steps. First, each of the 14 parameters (EC, pH, major and minor ions, and nutrients) receives a weight (W_i) depending on its relative importance on the general

water quality for drinking in Appendix A (Table A1). The steps for calculating the DWQI are estimated using Equations (2)–(5):

1. Consider the weights, W_i , for each element (i) of drinking water constituents; these weights can be changed from 1 (minimum value) to 5 (maximum value) and are assigned based on expert opinion. The corresponding weights utilized in this study are presented in Appendix A (Table A1).
2. Determine the relative weight, W_i , considering the number of elements (n):

$$W_i = \frac{w_i}{\sum_i^n w_i} \quad (2)$$

3. Calculate the quality rating scale (q_i) of each parameter [45]:

$$q_i = \frac{c_i}{s_i} \times 100 \quad (3)$$

where c_i is the i th chemical concentration in the considered water sample (mg/L); according to WHO standards, the sub-index of the i th parameter (SI_i) can be determined as follows (mg/L):

$$SI_i = W_i \times q_i \quad (4)$$

4. By calculating the SI_i for each parameter, the DWQI is determined using the following equation [46]:

$$DWQI_i = \sum_i^n SI_i \quad (5)$$

2.6. Human Health Risk Index (HHRI)

The health impact of water contaminated with toxic chemicals is checked based on the model developed by the US Environmental Protection Agency [33]. In this regard, risk assessment map of water resources might include important data to better address both qualitative and quantitative issues [47,48]. An HHRI describes the nature and likelihood of adverse health effects resulting from chemicals found in contaminated environmental media, which may be harmful to humans [49]. In general, there is a great deal of risk associated with oral exposure to the dermal and inhalation pathways of exposure. Accordingly, a non-carcinogenic pollutants health risk evaluation (e.g., NO_3^- and F^-) is carried out [50,51]. The US EPA provides a “Regional Screening Levels (RSLs) for Chemical Contaminants” online calculator [13]. HQ values greater than 1 suggest an increased risk of developing non-carcinogenic consequences throughout life. The exposure to F^- and NO_3^- in these groups is estimated using Equations (6) to (10) [33]:

$$CDI_{\text{Oral}} = \frac{(CW \times IR \times EF \times ED)}{(BW \times AT)} \quad (6)$$

$$HQ_{\text{Oral}} = \frac{CDI}{RfD_{\text{Oral}}} \quad (7)$$

$$CDI_{\text{Dermal}} = \frac{(CW \times CA \times K_p \times ET \times EF \times ED \times CF)}{(BW \times AT)} \quad (8)$$

$$HQ_{\text{Dermal}} = \frac{CDI}{RfD_{\text{Dermal}}} \quad (9)$$

$$HI_{\text{Total}} = \sum_{i=1}^n HQ_i \quad (10)$$

where CDI is the chronic daily intake through the oral pathway [$\text{mg}/(\text{kg} \times \text{day})$]; C represents the contaminant concentration (i.e., F^- and NO_3^-) in the water resources (mg/L); IR is the ingestion rate (L/day, $IR = 2.5$ L/day for adults, 0.78 L/day for Child); EF and ED are Exposure Frequencies (365 days/year) and Exposure Duration (standard exposure in the literature is suggested to be 30 years for adults and 12 years for children), respectively; BW

and AT are the average body weight (Kg, BW = 57.5 Kg and 18.7 Kg for adults and children, respectively) and the average exposure time (days, AT = 23,360 days and 4380 days for adults and children, respectively), respectively; and finally, HQ_i and RfD are the hazard quotient of ith pollutant and reference dose for non-carcinogenic contaminants, respectively. The RfD values for F^- and NO_3^- are 0.04 and 1.6 mg/(Kg × day), respectively [33]. HI is a hazard index that indicates the total non-carcinogenic risk. Non-carcinogenic risk values above 1 indicate health risks, while those below 1 indicate no health risks from drinking water containing toxic elements [33]. A detailed list of non-carcinogenic health risks can be found in Appendix A (Tables A2 and A3) Water resources containing high levels of NO_3^- and F^- may pose high health risks to humans if consumed for long periods as drinking and bathing water sources [13,52]. Thus, these two contaminants were considered in assessing non-carcinogenic risk for children and adults (i.e., Females and Males). More than 90% of the study region's population consumes untreated water resources for drinking. It was found that 55.81% and 65% of sampling points exceeded the prescribed levels of NO_3^- and F^- , respectively. Therefore, the consumption of such water in the region posed health risks to people of all ages.

According to Table 3, most samples fell within the F^- concentration range of 1–3 mg/L (38.33%), followed by 3–4 mg/L (6.6%). The number of samples greater than 4 also had a higher percentage (33%) in the Maku–Bazargan–Poldasht region, which may cause dental fluorosis and joint stiffness and brittleness in the region. NO_3^- concentrations of the samples showed that 21.6% of them were below the permissible limit, 25% were within the safe limit ($NO_3^- < 10$ mg/L), 58% were at health risk (NO_3^- : 10–50 mg/L), and 8.33% were at a high health risk (NO_3^- : 50–100 mg/L). Therefore, there was a very high health risk of NO_3^- (>100 mg/L) in 8.33% of samples, which causes methemoglobinemia in children (6 months old) and abortion in pregnant women [53].

Table 3. Classification of water resources based on F^- and NO_3^- (mg/L) HHRI.

	Corresponding Effects on Human Health Risk Assessment	Concentration (mg/L)	Station No.	% of the Samples
F^-	Safe limit	<1	3, 4, 6, 8, 11, 15, 19, 26, 30, 32, 42, 49, 57	21.6%
	Dental Fluorosis	1–3	7, 9, 10, 13, 14, 23, 24, 27, 28, 29, 31, 33, 37, 38, 39, 40, 41, 43, 47, 48, 53, 54, 60	38.3%
	Stiff and fragile Bones/Joints	3–4	1, 17, 25, 59	6.6%
	Defects in knees; crippling fluorosis; bones conclusively paralyzed resulting in incapability to walk or stand straight	>4	2, 5, 12, 16, 18, 20, 21, 22, 34, 35, 36, 44, 45, 46, 50, 51, 52, 55, 56, 58	33%
NO_3^-	Safe limit	<10	4, 5, 8, 11, 12, 15, 19, 20, 26, 27, 28, 30, 32, 36, 49	25%
	Health risk	10–50	1, 2, 3, 9, 10, 13, 14, 17, 21, 22, 23, 24, 25, 29, 31, 33, 34, 35, 37, 40, 42, 43, 44, 45, 46, 47, 48, 50, 51, 52, 55, 56, 58, 59, 60	58%
	High health risk	50–100	7, 38, 41, 54, 57	8.3%
	Very high health risk	>100	6, 16, 18, 39, 53	8.3%

2.7. Information- Fusion

In accordance with Esteban et al. [54], it is essential to formulate a strategy in advance of engaging in any undertaking of information fusion to assist in solving the problem efficiently and robustly. Data fusion architecture is a platform that connects databases with the help of data fusion techniques to create an integrated system. It is a mathematical model that functions as the basis for merging data from several sources into one. This methodology is based on goals and combines low- and high-level information. This term refers to a variety of methods and approaches used to combine information to enhance quality, reduce uncertainty, or uncover novel knowledge or characters from the collected data. Theoretically, information fusion combines data from a number of diverse data sources [11]. Typically, it can be characterized at the signal level, the pixel level, the feature

level, or the Top level [55], each with its own definitions and associated procedures. There is also another way of categorizing fusion in terms of top-level, medium-level, and high-level fusions [56]. Several techniques support information fusion, including statistical matching, grey relational analysis, moving average filters, and Bayesian inference [2,57].

3. Results and Discussion

3.1. Statistical Analysis

Table 2 gives a comprehensive statistical summary of the various physicochemical parameters (EC, pH, Ca^{2+} , Mg^{2+} , Na^+ , K^+ , NH_4^+ , Cl^- , Br^- , SO_4^{2-} , NO_2^- , NO_3^- , and F^-) as well as their comparison with the drinking water quality limits set by US EPA for 60 water samples. The main factors contributing to the significant F^- concentration in water resources are low velocity, rock chemistry, long water–rock interactions [58], and high HCO_3^- and Na^+ concentrations. There was a positive correlation between F^- concentrations and the values of HCO_3^- , Na^+ , and K^+ concentrations, according to the correlation analysis (Table 4). Groundwater with dominant HCO_3^- , Na^+ , and K^+ concentrations originated from igneous rocks [59], so the correlation indicates that excessive F^- ion concentrations may have resulted from fluorine-bearing minerals associated with the source volcanic rocks as well as the application of fertilizers and pesticides on the field [60,61]. Generally, most ions were positively correlated with Cl^- , and particularly Na^+ , Mg^{2+} , and SO_4^{2-} showed a strong correlation with Cl^- , suggesting that they came from the same origin of saline water [62], meaning they are furthermore representative of a high occurrence of chemical weathering and the subsequent leaching of secondary salts. Chemical weathering, anthropogenic impacts, and salt leaching were the main factors contributing to the Cl^- contamination in the study area. The correlation of F^- and the other ions showed that it is poorly correlated with Ca^{2+} and Mg^{2+} and positively correlated with Na^+ , K^+ , and HCO_3^- . It can therefore be concluded that high F^- concentrations exist in water with low Ca^{2+} and Mg^{2+} levels, as well as in water with high Na^+ levels. Low Ca^{2+} resulted from the intense cation exchange reaction between Na^+ and Ca^{2+} . The presence of a high HCO_3^- and an alkaline pH in the samples resulted in the precipitation of Mg^{2+} as Dolomite and Ca^{2+} as Calcite. According to Sarma and Rao [63], this process leads to a higher concentration of Na^+ in water resources. It is evident that HCO_3^- is highly correlated with F^- , indicating that volcanic rock weathering is the major cause of F^- formation [60]. Low levels of Ca^{2+} and Mg^{2+} in the groundwater within the area may be contributing to high concentrations of F^- in the water resources.

Table 4. Correlation matrix between the hydrochemical variables in the Maku–Bazargan–Poldasht area.

	EC	pH	Na^+	NH_4^+	K^+	Ca^{2+}	Mg^{2+}	F^-	Cl^-	NO_2^-	Br^-	NO_3^-	SO_4^{2-}	HCO_3^-
EC	1													
pH	−0.27	1												
Na^+	0.95 **	−0.29 *	1											
NH_4^+	0.45 **	−0.23 *	0.56 **	1										
K^+	0.66 **	−0.29 *	0.73 **	0.22	1									
Ca^{2+}	0.87 **	−0.31 *	0.76 **	0.25	0.63 **	1								
Mg^{2+}	0.91 **	−0.25	0.82 **	0.33	0.56 **	0.85 **	1							
F^-	0.38 **	−0.16	0.52 **	0.41 **	0.46 **	0.18	0.16	1						
Cl^-	0.75 **	−0.44 **	0.72 **	0.33 *	0.44 **	0.71 *	0.65 **	0.40 **	1					
NO_2^-	−0.09	−0.04	−0.09	−0.006	−0.07	−0.11 *	−0.06	0.04	−0.08	1				
Br^-	0.33 **	−0.08	0.39 **	0.25	0.27 *	0.13	0.18	0.35 **	0.15	−0.07	1			
NO_3^-	0.26 *	−0.30 *	0.17	−0.16	0.22	0.26 *	0.35 **	−0.06	0.34 **	−0.003	−0.04	1		
SO_4^{2-}	0.30 *	−0.009	0.25 *	0.02	0.19	0.34 **	0.31 *	0.04	0.31 *	−0.07	−0.01	0.05	1	
HCO_3^-	0.25 *	−0.35 **	0.37 **	0.26 *	0.36 **	0.05	0.04	0.71 **	0.35 **	−0.09	0.17	−0.05	−0.07	1

Notes: ** Correlation = significant at the level 0.01 (2-tailed). * Correlation = significant at the level 0.05 (2-tailed).

3.2. Factor Analysis (FA)

Factor analysis (FA) is a method that has been successfully used by different authors for the assessment of water quality and chemistry [64], since it helps in the distribution analysis as well as in tracing the source(s) of the chemical components in water [65]. The factor analysis for the physicochemical parameters in the water resources of the Maku–Bazargan–Poldasht region is given in Table 5. A total of four components were extracted based on the results of the FA analysis, which accounted for 81.83% of the variance in the data. A rotating factor matrix for the parameters studied can be found in Table 5. The interpretability of the factor loads without rotation is difficult, so in order to make the factors more interpretable, the factors were rotated. The results showed that the FA1 described 35.86%, the FA2 described 18.07%, the FA3 described 10.45%, and the FA4 described 7.51% of the total variance. With a variance of 35.86%, FA1 was positively and considerably related to EC, Na⁺, K⁺, Ca²⁺, Mg²⁺, Cl⁻, and SO₄²⁻ concentrations. These associations indicated: (i) the interaction between water and rocks in the study area; and (ii) the general trend of dissolution in waters within the study area. This interaction was unlimited to one site, but rather the flow through the aquifer encouraged the tendency for further interactions and the dissolution process to occur in the future. With a total variance of 18.07%, FA2 can be associated with the concentration of F⁻ and HCO₃⁻, and F⁻ anomalies resulted predominantly from geogenic processes. The F⁻ concentration in the samples with a high HCO₃⁻ concentration was higher than those with a low HCO₃⁻ concentration. The FA3, with a total variance of 10.4%, correlated well with pH and Br⁻ concentrations, and the existence of NO₃⁻ with negative loading indicated anoxic conditions in the study area [66], and denitrification and NO₃⁻ reduction are related geochemically [67]. A major source of anthropogenic NO₃⁻ and nitrite is artificial fertilizers, and various industrial processes also produce NO₃⁻ in their waste streams. In this study, the spatial distributions of nitrate, nitrite, and ammonium were investigated. High-NO₃⁻, low-NO₂⁻, and high-NH₄⁺ water resources were observed. The proportions of high-NO₃⁻ and high-NH₄⁺ water resources in urbanized areas were nearly or more than twice those in non-urbanized areas (Figure 6). High NO₃⁻ levels in the Maku–Bazargan–Poldasht aquifers probably originated mainly from industrialization accompanied by wastewater leakage. Urbanization accompanied by the leakage of domestic sewage, is likely to be another main driving force for high NO₃⁻ levels in the water resources. The high loading of NO₃⁻ ions indicated that there was anthropogenic input to the system via the leaching of fertilizers from farming regions, which is linked to the interaction of surface water with the geological formations in the area. The element Br⁻ can originate from old rivers and seas, as well as from animal waste, which can have a profound impact on water supply quality and create contaminations that are mainly caused by the impact of human activities related to farming, with slight influences from domestic sewage. The total variance of 7.51% can be attributed to the FA4, which is related to the concentration of NO₂⁻.

Table 5. Results of factor loading based on factor analysis of the samples in the Maku–Bazargan–Poldasht area.

Parameters	Factor 1	Factor 2	Factor 3	Factor 4
EC	0.94	0.23	0.032	0.026
pH	−0.2	−0.44	0.62	−0.22
Na ⁺	0.87	0.42	0.12	0.046
NH ₄ ⁺	0.38	0.41	0.37	0.3
K ⁺	0.64	0.40	−0.05	−0.10
Ca ²⁺	0.91	0.023	−0.13	−0.03
Mg ²⁺	0.93	−0.006	−0.081	0.049
F ⁻	0.22	0.82	0.23	−0.02
Cl ⁻	0.74	0.34	−0.23	−0.003
NO ₂ ⁻	−0.08	−0.11	−0.06	0.87

Table 5. Cont.

Parameters	Factor 1	Factor 2	Factor 3	Factor 4
Br ⁻	0.28	0.27	0.55	-0.07
NO ₃ ⁻	0.32	-0.06	-0.67	-0.08
SO ₄ ²⁻	0.50	-0.23	0.068	-0.23
HCO ₃ ⁻	0.029	0.90	-0.058	-0.085
% of Variance	35.86	18.07	10.45	7.51
Cumulative %	35.86	53.93	64.39	71.9

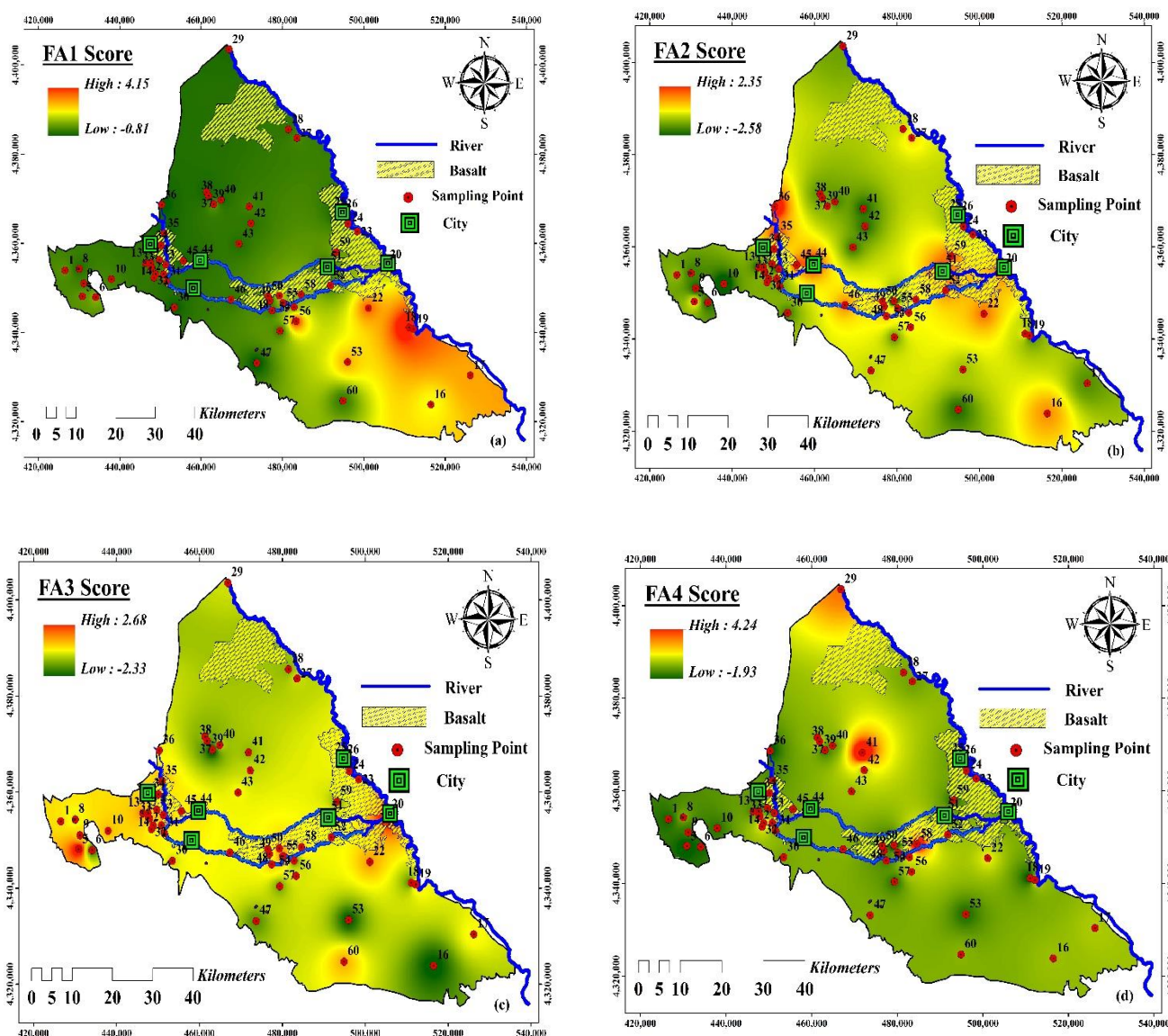


Figure 6. Spatial distribution of factors scores for the Maku–Bazargan–Poldasht area: (a) Factor 1 (FA1), (b) Factor 2 (FA2), (c) Factor 3 (FA3), (d) Factor 4 (FA4).

3.3. DWQI

The DWQI was employed to assess the status of the water resource quality for drinking water objects in the Maku–Bazargan–Poldasht area. Unlike previous studies on water quality, which used a common classification for drinking purposes, this study determined the ranges between excellent and unsuitable water quality based on a rational classification. As a result, the DWQI was classified as belonging to the excellent water quality class if

it was smaller than the minimum data utilized to calculate the Drinking Water Quality Index; the good water quality class if it was among US EPA standards and the average of the data used; the poor quality class if it ranged from the safe limit to the average data; and the unsuitable class if the results of calculating the drinking water index were between the average to maximum data. The calculated DWQI ranged from 51.19 to 2200, with a mean of 502.71. In total, 28 samples (46%) were classified as poor and 22 samples (36%) as unsuitable in terms of their quality, while the remaining 10 samples were classified as good for drinking (Table 6). The water samples were analyzed for F^- and NO_3^- concentrations and then the rational (i.e., proposed classification) and conventional DWQI values were calculated as follows: (i) classify the concentrations of NO_3^- and F^- into three categories: safe (<10 mg/L), health risk (10–50 mg/L), and high health risk (>50 mg/L), and safe (<1 mg/L), dental fluorosis (1–4 mg/L), and defects in knees—crippling fluorosis (>4 mg/L), respectively; (ii) classify the DWQI (conventional–rational) into “Good”, “Poor”, and “Unsuitable” bands; (iii) assign a ‘3’ to a given index performance at the samples if the difference in the categories of F^- - NO_3^- concentration and the DWQI value is 0 but assign scores of two or one when the differences are one or two, respectively; and (iv) add the scores for the DWQI and calculate their Correlation Index (CI). Consider the following example for obtaining the CI for the prediction rational (proposed classification) DWQI. The results showed that there were 38 and 30 samples for the same class, 19 and 24 samples with a difference of one in the categories of the F^- -DWQI and nitrate-DWQI values, respectively, and 3 and 6 with a difference of two in the categories of the F^- -DWQI and nitrate-DWQI values, respectively. A higher CI means a higher correlation. The coincidence of the water samples (the F^- - NO_3^- concentration) and the predicted DWQI categories are presented in Table 6. Ultimately, this indicated that a higher percentage of the water samples from the study region were unsuitable in terms of quality. The spatial distribution of the DWQI (Figure 7) showed that the east and southeast of the area had a high DWQI compared to the north and west of the Maku–Bazargan–Poldasht area. The water quality along the Zangmar and Sari Su rivers has deteriorated in recent years, and the worst quality for drinking occurred at the confluence of the two rivers with the Aras River.

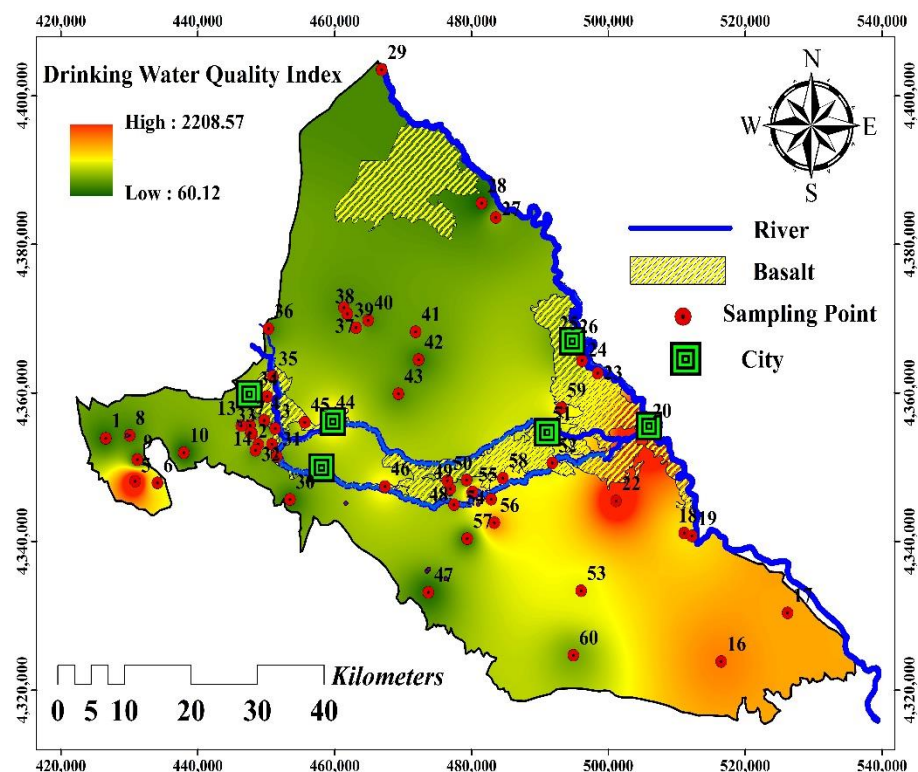


Figure 7. Drinking Water Quality Index map of the Maku–Bazargan–Poldasht area.

Table 6. Non-carcinogenic HR for adults and children as well as DWQI and corresponding water quality classification of the samples and Correlation Index (CI) between Drinking Water Quality Indices (conventional–rational) and F^- - NO_3^- levels at the water samples.

Samples	Non-Carcinogenic			DWQI Classify		Samples	Non-Carcinogenic			DWQI	
	Adults	Child	Value	Conventional	Rational (Proposed Classification)		Adults	Child	Value	Conventional	Rational (Proposed Classification)
1	3.73	3.57	102.2	Poor	Poor	31	1.67	1.78	209.2	Unsuitable	Poor
2	5.17	4.54	1057.5	Unsuitable	Unsuitable	32	0.96	0.9	167.3	Poor	Poor
3	0.84	0.97	100.8	Poor	Good	33	1.33	1.35	235.2	Unsuitable	Poor
4	0.47	0.48	150.1	Poor	Poor	34	4.72	4.14	506.9	Unsuitable	Poor
5	3.79	3.27	1812.9	Unsuitable	Unsuitable	35	6.56	5.71	518	Unsuitable	Poor
6	4.83	6.39	636.2	Unsuitable	Unsuitable	36	8.01	6.92	213	Unsuitable	Poor
7	3.16	3.42	268.7	Unsuitable	Poor	37	1.99	2.23	211.9	Unsuitable	Poor
8	0.64	0.60	104.5	Poor	Good	38	3.57	4.10	263.8	Unsuitable	Poor
9	1.37	1.34	64.9	Good	Good	39	4.63	5.90	343.9	Unsuitable	Poor
10	1.62	1.63	69.6	Good	Good	40	1.87	2.12	205.06	Unsuitable	Poor
11	0.31	0.26	695.7	Unsuitable	Unsuitable	41	2.81	3.16	296	Unsuitable	Poor
12	3.72	3.20	1576.7	Unsuitable	Unsuitable	42	1.49	1.71	160.6	Poor	Poor
13	1.69	1.61	335.5	Unsuitable	Poor	43	2.22	2.27	245.6	Unsuitable	Poor
14	1.55	1.54	252.7	Unsuitable	Poor	44	6.64	5.85	877.1	Unsuitable	Unsuitable
15	0.65	0.66	51.1	Good	Good	45	4.80	4.22	578.5	Unsuitable	Unsuitable
16	7.35	8.44	971.8	Unsuitable	Unsuitable	46	4.49	4.23	679.7	Unsuitable	Unsuitable
17	3.71	3.78	871.9	Unsuitable	Unsuitable	47	1.26	1.30	109	Poor	Good
18	7.41	7.65	707.14	Unsuitable	Unsuitable	48	2.29	2.11	392.8	Unsuitable	Poor
19	0.47	0.48	714.7	Unsuitable	Unsuitable	49	0.76	0.71	330.5	Unsuitable	Poor
20	3.79	3.27	2211.3	Unsuitable	Unsuitable	50	4.20	3.86	513.4	Unsuitable	Poor
21	4.01	3.75	1171.6	Unsuitable	Unsuitable	51	5.79	5.16	443.7	Unsuitable	Poor
22	7.01	6.38	1475.2	Unsuitable	Unsuitable	52	3.63	3.34	579.8	Unsuitable	Unsuitable
23	1.24	1.23	352.8	Unsuitable	Poor	53	5.62	6.67	588.4	Unsuitable	Unsuitable

Table 6. Cont.

Samples	Non-Carcinogenic			DWQI Classify		Samples	Non-Carcinogenic			DWQI	
	Adults	Child	Value	Conventional	Rational (Proposed Classification)		Adults	Child	Value	Conventional	Rational (Proposed Classification)
24	1.52	1.57	233	Unsuitable	Poor	54	3.90	4.50	627.4	Unsuitable	Unsuitable
25	3.07	2.85	332.6	Unsuitable	Poor	55	7.36	6.5	724.05	Unsuitable	Unsuitable
26	0.65	0.65	105.3	Poor	Good	56	4.07	3.77	987.5	Unsuitable	Unsuitable
27	1.47	1.34	354.3	Unsuitable	Poor	57	2.67	3.35	109.8	Poor	Good
28	1.08	1.00	65	Good	Good	58	3.94	3.57	695.6	Unsuitable	Unsuitable
29	1.55	1.54	221.2	Unsuitable	Poor	59	3.92	3.89	655.4	Unsuitable	Unsuitable
30	0.65	0.66	101.3	Poor	Good	60	1.61	1.73	338.8	Unsuitable	Poor

Index	Class	NO ₃ ⁻ concentration			CI	F ⁻ concentration			CI
		Safe (<10 mg/L)	Health Risk (10–50 mg/L)	High Health Risk (>50 mg/L)		Safe (<1 mg/L)	Florsis (Dental–Bones) (1–4 mg/L)	Defects in knees; crippling fluorosis (>4 mg/L)	
Rational (proposed classification)	Good	3	5	5	144	4	6	3	155
	Poor	4	21	11		4	19	4	
	Unsuitable	1	4	6		0	5	15	
Conventional	Good	2	4	7	94	1	8	4	139
	Poor	2	5	29		3	2	22	
	Unsuitable	0	1	10		0	0	20	

Note: # HR: Health Risk.

3.4. Non-Carcinogenic Health Risk Assessment

A non-carcinogenic hazard is mainly associated with the consumption of portable water and contact with the skin. Three factors influence the CDI values: the concentration of the contaminants, the rate at which the water is ingested, and the individual’s body weight. The CDI values in children are comparatively higher than those in adults. The child’s HQ oral intake values range from 0.27 to 6.82, and the adult’s HQ oral intake ranges from 0.31 to 7.95 (with an average of 2.94). In the case of children, the dermal intake ranges from 0.002 to 1.7, and in the case of adults, the oral intake ranges from 0.001 to 0.96 (with an average of 0.18). The spatial distribution of human health risk for both children and adults (Figure 8) along the study area indicates that high HI values (i.e., high HHR) prevail in the southeast and patches in the west.

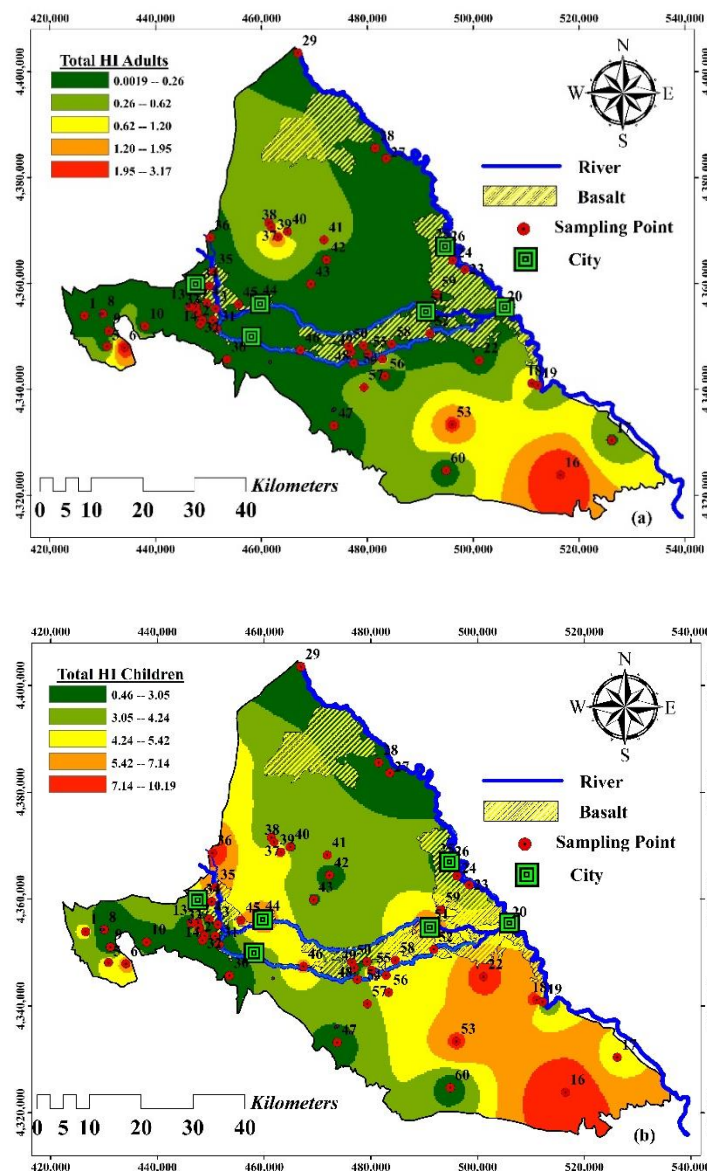


Figure 8. Spatial distribution of non-carcinogenic HHRA for (a) adults and (b) children.

Health risks were assessed using the model developed by the US EPA to assess the health risks related to this study area. A summary of the calculated results of the non-carcinogenic health risks posed by NO_3^- and F^- contaminations through the pathways of drinking water contamination for adults and children is explicitly presented in Table 6 and Figure 9. It summarizes both the oral intake and dermal intake of each of the different

groups of inhabitants in the studied region, as well as the total hazard index (THI) corresponding to each group of inhabitants. In children and adults, the HQ values ranged from 0.002 to 1.7 and 0.0013 to 3.2, respectively, depending on the dermal pathway. The mean dermal contact values for children and adults were 0.32 and 0.18, respectively. The hazard index values for children and adults ($HQ_{Oral} + HQ_{Dermal} = HI$) ranged from 0.000014 to 7.2 for children and from 0.000062 to 3.2 for adults. The body weight of a child is lower than that of an adult. The estimated hazard quotient for children is higher than for adults. Non-carcinogenic risks to children in this region were higher than those for adults. The mean values for all the groups of people (i.e., children and adults) were, however, within the allowable limits ($HI < 1$) [53]. Since most samples present a high level of non-carcinogenic risks, they are not suitable for direct consumption. According to the results, the majority of the samples were not fit for human consumption, as they posed unacceptable health risks to both adults and children alike. Children are at an increased risk when compared to adults. Through the ingestion pathway, infants are the most vulnerable group of people. It is evident from the hazard index that the majority of the samples (i.e., 72% and 60%) may pose a risk to adults and children, respectively. There is a need to take immediate remedial steps in this region to prevent the residents from being exposed to NO_3^- and F^- through ingestion. Moreover, the results of the total risk via ingestion and dermal contact showed that ingestion was the predominant pathway. Different strategies can be used to reduce the risk of dental fluorosis, including (a) the use of alternative water sources, (b) improving nutrition, and (c) the defluoridation of water. The defluoridation methods can be divided into adsorption ([68–72]), participation/coagulation [73], electrocoagulation [74–78], nanofiltration [79,80], and nanofiltration [81]. In addition, F^- -resistant bacteria play a crucial role in the bioremediation and biotransformation of anions in order to convert them into less available and less harmful forms.

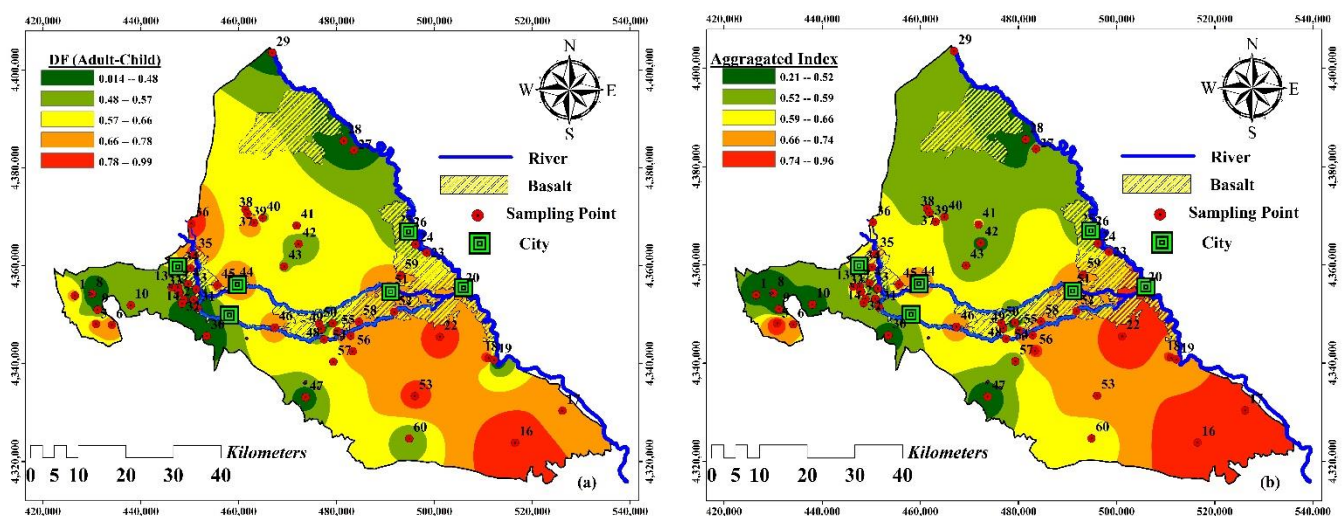


Figure 9. Spatial distribution (a) data fusion of HHRI results (Strategy 1); (b) comprehensive risk maps (Strategy 2).

3.5. Data Fusion

The main data integration objectives in this research are: (i) refining data and improving data quality; (ii) inventing additional inferences and rising advantage from data; (iii) improving understanding and decisions. To incorporate datasets from numerous sources, specialized data fusion techniques can be incorporated into the HHRI framework recommended earlier by the National Academy of Sciences [82]. In this study, information

fusion was performed in order to combine index values by DWQI and HHRI indicators to produce a comprehensive risk map, a scheme depicted in and outlined below [83],

$$DF_1 = \left[\frac{\sqrt[2]{HI_{Adult}} + \sqrt[3]{HI_{Child}}}{2} \right] \quad (11)$$

$$DF_{Total} = \left[\frac{\sqrt[3]{DWQI} + \sqrt[2]{THI}}{2} \right] \quad (12)$$

The data-fused HI (i.e., aggregating HI for both children and adults) values ranged between 0.01 and 0.99 in the Maku–Bazargan–Poldasht area. The spatial distribution of the fused Health Index (Figure 9a) shows that the water resources of the southeast regions had a greater health hazard, followed by the west of the area.

Total data-fused HI values varied from 0.21 to 0.96. Based on the aggregated HI (i.e., combining the DWQI and data-fused HI at Strategy 1), the southeast of the area bore the highest risk to the people consuming water. On the other hand, it was observed that aggregating the DWQI to HI may decrease the health risk in the central parts of the Maku–Bazargan–Poldasht area, even though there is a greater risk in Strategy 1 than in Strategy 2. The aggregated index was compiled from the information from Strategy 1 by implementing an unsupervised learning plan, which is shown to capture information on the adverse water quality and health risks associated with water of poor quality.

4. Performance Metrics

The Area Under Curve (AUC) and Receiver Operating Characteristic (ROC) curve can be utilized to measure the accuracy of a diagnostic system [84]. They were recently used to evaluate a groundwater vulnerability map accuracy by [18]. The events related to diagnosis can be clustered into four groups, including True Positive (TP), False Positive (FP), True Negative (TN), and False Negative (FN). The ROC curve plots of FP versus TP show that desirable performance has a deviation towards the upper left corner of this curve. The AUC quantifies this as the ratio of the area under the ROC curve to the whole area that varies between 0.5 to 1. The AUC values 0.5 and 1 mean poor and perfect performance, respectively. The area under the curve is used as one of the error estimation methods; whenever the AUC is close to one, the model has high accuracy. Table 7 presents the AUC values of both Strategy 1 and Strategy 2. The AUC value is improved from Strategy 1 (0.92) to Strategy 2 (0.98). Figure 10 shows the ROC curves for both strategies obtained by drawing TPR (sensitivity) versus FPR (one—specificity). As shown in Figure 10, Strategy 2 has the highest level under the curve and has the highest accuracy. These results provide evidence of the feasibility of aggregated indices.

Table 7. Performance metrics to evaluate different water quality assessment strategies.

Test Result Variable(s)	Area	Std. Error ^a	Asymptotic Sig. ^b	95% Confidence Interval	
				Lower Bound	Upper Bound
Strategy 1	0.92	0.003	0.00	0.92	0.93
Strategy 2	0.98	0.001	0.00	0.97	0.98

Notes: the test result variable(s): Strategy 1 and Strategy 2 have at least one tie between the positive and negative actual state group. Statistics may be biased. ^a Under the nonparametric assumption. ^b Null hypothesis: true area = 0.5.

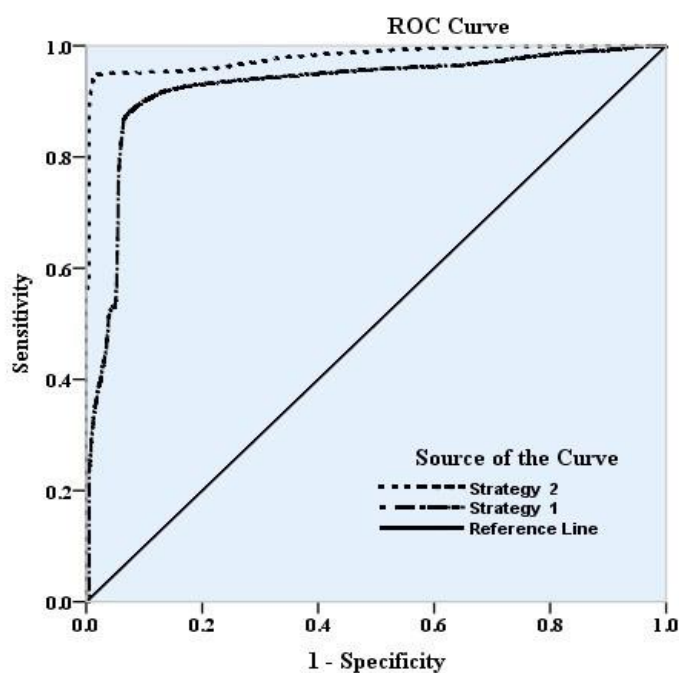


Figure 10. The ROC curves for Strategies.

5. Conclusions

This study evaluated water quality and human health risks, considering the hydrogeological and hydrochemical properties of Maku–Bazargan–Poldasht, Iran. The water quality analysis showed that F^- and NO_3^- concentrations were higher than the permissible level for drinking. A multivariate analysis combining factor analysis and correlations revealed that both geogenic and anthropogenic agents significantly impacted the quality of the water resources in the study area. Using the US EPA water quality standards for elements in drinking water, this study modified the water quality index classes for the first time. The DWQI results indicated that most of the study area fell within poor or inopportune drinking water conditions. Based on the calculation of the CI and the comparison of the assessment of drinking water quality as well as the accurate determination of suitable and unsuitable areas with the rational (proposed classification) and conventional classification, the results indicated that rational classifications for drinking water quality indicators and the definition of drinking water quality categories were more accurate than conventional classifications. Health risk results demonstrated a considerable non-carcinogenic health risk due to high NO_3^- and F^- exposure through drinking water. Children were found more defenseless than adults in the age categories. A fusion model based on the DWQI and HHRI was developed for fast safety control of residues related to water quality and health. The northwest, southeast and central portions of Maku–Bazargan–Poldasht were considered to be the most unsafe regions in the study area. A high level of NO_3^- and NH_4^+ pollution occurred in the study area, and since there is no effective control and treatment in such a rapidly urbanized region, this process is bound to get worse in the future. For newly and old-urbanized areas, especially in developing countries, there is a need for the long-term monitoring of NO_3^- and NH_4^+ in the area's water resources. These results suggest that the governing bodies require immediate intervention in these areas. Furthermore, the obtained results showed that alternate preparations should be made for drinking water sources, and people must be aware of the water quality they consume in the affected areas.

Author Contributions: Conceptualization, A.A.N.; methodology, R.B.; software, Z.S.; validation, A.A.N. and M.R.N.; formal analysis, Z.S.; investigation, and resources, R.B.; data curation, Z.S.; writing—original draft preparation, Z.S.; writing—review and editing, M.R.N.; visualization, M.R.N.; supervision, A.A.N.; project administration, M.R.N.; funding acquisition, A.A.N. All authors have read and agreed to the published version of the manuscript.

Funding: This research received no external funding.

Data Availability Statement: The study did not report any data.

Acknowledgments: The authors would like to thank the Center for International Scientific Studies and Collaboration (CISSC), Ministry of Science, Research and Technology, for their support with this research.

Conflicts of Interest: The authors declare no conflict of interest.

Appendix A

Table A1. Weight and relative weight of each parameter compared with US EPA standard.

Parameter	Unit	US EPA	Weight (w_i)	Weight for DWQI
EC	($\mu\text{S}/\text{cm}$)	1000	3	0.068
pH	-	7.5	3	0.068
Na ⁺	(mg/L)	200	3	0.068
NH ₄ ⁺	(mg/L)	0.05	4	0.09
K ⁺	(mg/L)	12	2	0.045
Ca ²⁺	(mg/L)	200	2	0.045
Mg ²⁺	(mg/L)	30	2	0.045
F ⁻	(mg/L)	1.5	5	0.11
Cl ⁻	(mg/L)	250	3	0.068
NO ₂ ⁻	(mg/L)	3	4	0.09
Br ⁻	(mg/L)	0.1	3	0.068
NO ₃ ⁻	(mg/L)	10	5	0.11
SO ₄ ²⁻	(mg/L)	250	3	0.068
HCO ₃ ⁻	(mg/L)	300	2	0.045
Total Weight			44	1

Table A2. Definitions, symbols, units, and values associated with equations used for health risk assessment.

P	Meaning	Unit	Oral Values		Dermal Values		References
			(Adults)	(Children)	(Adults)	(Children)	
AT	Average exposure time for ingestion	Days	25,550	3650	Non-carcinogenic effects = ED × 365 = 10950 (Adults). Carcinogenic effects AT = 70 × 365 = 25,550	2190 (Child). Carcinogenic effects AT = 70 × 365 = 25,550	[33,85]
BW	Average body Weight of a population group	Kg	70	25	70	25	[33]
CF	Conversion factor	L/cm ³			1.1000		[85]
CDI	Chronic daily intake	$\mu\text{g}/\text{kg}/\text{day}$	-	-	-	-	[85]
CW	Concentration in water	$\mu\text{g}/\text{L}$	-	-	-	-	Study data
ED	Exposure Duration through ingestion	year	70	10	30	6	[33]

Table A2. Cont.

P	Meaning	Unit	Oral Values		Dermal Values		References
			(Adults)	(Children)	(Adults)	(Children)	
EF	Dermal exposure frequency	days/year	365	350	[33]		
ET	Exposure time in the shower	h/event	-	-	0.58	1	[33]
IR	Daily groundwater ingestion rate	L/day	2.2	1	-	-	[85]
Kp	Dermal permeability coefficient	cm/h			Al(0.001), As(0.001), Cr(0.003), Cu(0.001), Fe(0.001), Mn(0.001), Ni(0.004), Pb(0.001), Zn(0.0006), Cd(0.001)	[33]	
SA	Exposed skin area during bathing	cm ²	-	-	18,000	6600	[33]

Table A3. Dermal permeability coefficient, reference dose, slope factor, and gastrointestinal absorption coefficient for each element.

Elements	Units	Non-Carcinogen		Carcinogen
		Oral RfD (µg/Kg/day)	Dermal RfD (µg/Kg/day)	SF (kg × day/mg)
F ⁻	(µg/L)	0.04 [33]	60 [33]	Not Determined
NO ₃ ⁻	(µg/L)	1.6 [33]	0.025 [33]	Not Determined

References

- Yeşilnacar, İ.M.; Yetiş, A.D.; Dülgergil, C.T.; Kumral, M.; Atasoy, A.D.; Rastgeldi Doğan, T.; Tekiner, İ.S.; Bayhan, I.; Aydoğdu, M. Geomedical assessment of an area having high-fluoride groundwater in southeastern Turkey. *Environ. Earth Sci.* **2016**, *75*, 162. [CrossRef]
- Li, C.; Gao, X.; Wang, Y. Hydrogeochemistry of high-fluoride groundwater at Yuncheng Basin, northern China. *Sci. Total Environ.* **2015**, *508*, 155–165. [CrossRef] [PubMed]
- Ganyaglo, S.Y.; Gibrilla, A.; Teye, E.M.; Owusu-Ansah, E.D.-G.J.; Tettey, S.; Diabene, P.Y.; Asimah, S. Groundwater fluoride contamination and probabilistic health risk assessment in fluoride endemic areas of the Upper East Region, Ghana. *Chemosphere* **2019**, *233*, 862–872. [CrossRef]
- Elumalai, V.; Nwabisa, D.P.; Rajmohan, N. Evaluation of high fluoride contaminated fractured rock aquifer in South Africa—Geochemical and chemometric approaches. *Chemosphere* **2019**, *235*, 1–11. [CrossRef] [PubMed]
- Harvard. Fluoride-Childrens-Health-Grandjean-Choi. Available online: <http://www.hsph.harvard.edu/news/features/> (accessed on 4 February 2015).
- Aslani, H.; Zarei, M.; Taghipour, H.; Khashabi, E.; Ghanbari, H.; Ejlali, A. Monitoring, mapping and health risk assessment of Fluoride in drinking water supplies in rural areas of Maku and Poldasht, Iran. *Environ. Geochem. Health* **2019**, *41*, 2281–2294. [CrossRef]
- Chen, J.; Wu, H.; Qian, H.; Gao, Y. Assessing nitrate and Fluoride contaminants in drinking water and their health risk of rural residents living in a semiarid region of northwest china. *Expo. Health* **2017**, *9*, 183–195. [CrossRef]
- Adimalla, N. Controlling factors and mechanism of groundwater quality variation in semiarid region of South India: An approach of water quality index (WQI) and health risk assessment (HRA). *Environ. Geochem. Health* **2020**, *42*, 1725–1752. [CrossRef] [PubMed]
- Nieuwenhuijsen, M.; Paustenbach, D.; Duarte-Davidson, R. New developments in exposure assessment: The impact on the practice of health risk assessment and epidemiological studies. *Environ. Int.* **2006**, *32*, 996–1009. [CrossRef] [PubMed]
- Dyck, R.; Islam, M.S.; Zargar, A.; Mohapatra, A.; Sadiq, R. Application of data fusion in human health risk assessment for hydrocarbon mixtures on contaminated sites. *Toxicology* **2013**, *313*, 160–173. [CrossRef]
- See, L.; Abrahart, R. Multi-model data fusion for hydrological forecasting. *Comput. Geosci.* **2001**, *27*, 987–994. [CrossRef]
- Nadiri, A.A.; Fijani, E.; Tsai, F.T.-C.; Moghaddam, A.A. Supervised committee machine with artificial intelligence for prediction of fluoride concentration. *J. Hydroinform.* **2013**, *15*, 1474–1490. [CrossRef]

13. Yousefi, M.; Ghoochani, M.; Mahvi, A.H. Health risk assessment to Fluoride in drinking water of rural residents living in the Poldasht city, Northwest of Iran. *Ecotoxicol. Environ. Saf.* **2018**, *148*, 426–430. [[CrossRef](#)] [[PubMed](#)]
14. Li, P.; He, X.; Guo, W. Spatial groundwater quality and potential health risks due to nitrate ingestion through drinking water: A case study in Yan'an City on the Loess Plateau of northwest China. *Hum. Ecol. Risk Assess.* **2019**, *25*, 11–31. [[CrossRef](#)]
15. Nadiri, A.A.; Sedghi, Z.; Khatibi, R. Qualitative risk aggregation problems for the safety of multiple aquifers exposed to nitrate, fluoride and arsenic contaminants by a 'Total Information Management' framework. *J. Hydrol.* **2021**, *595*, 126011. [[CrossRef](#)]
16. Asghari Moghaddam, A.; Fijani, E. Hydrogeologic framework of the Maku area basalts, northwestern Iran. *Hydrogeol. J.* **2009**, *17*, 949–959. [[CrossRef](#)]
17. Mahvi, A.H.; Ghanbarian, M.; Ghanbarian, M.; Khosravi, A.; Ghanbarian, M. Determination of Fluoride concentration in powdered milk in Iran 2010. *Br. J. Nutr.* **2010**, *107*, 1077–1079. [[CrossRef](#)]
18. Nadiri, A.A.; Sedghi, Z.; Khatibi, R.; Gharekhani, M. Mapping vulnerability of multiple aquifers using multiple models and fuzzy logic to objectively derive model structures. *Sci. Total Environ.* **2017**, *593–594*, 75–90. [[CrossRef](#)]
19. Nadiri, A.A.; Sedghi, Z.; Khatibi, R.; Sadeghfam, S. Mapping specific vulnerability of multiple confined and unconfined aquifers by using artificial intelligence to learn from multiple DRASTIC frameworks. *J. Environ. Manag.* **2018**, *227*, 415–428. [[CrossRef](#)]
20. Kamarehie, B.; Jafari, A.; Zarei, A.; Fakhri, Y.; Ghaderpoori, M.; Alinejad, A. Non-carcinogenic health risk assessment of nitrate in bottled drinking waters sold in Iranian markets: A Monte Carlo simulation. *Accredit. Qual. Assur.* **2019**, *24*, 417–426. [[CrossRef](#)]
21. Adimalla, N.; Qian, H. Groundwater chemistry, distribution and potential health risk appraisal of nitrate enriched groundwater: A case study from the semi-urban region of South India. *Ecotoxicol. Environ. Saf.* **2021**, *207*, 111277. [[CrossRef](#)]
22. Ravindra, K.; Thind, P.S.; Mor, S.; Singh, T.; Mor, S. Evaluation of groundwater contamination in Chandigarh: Source identification and health risk assessment. *Environ. Pollut.* **2019**, *255*, 113062. [[CrossRef](#)] [[PubMed](#)]
23. Jha, M.K.; Shekhar, A.; Jenifer, M.A. Assessing groundwater quality for drinking water supply using hybrid fuzzy-GIS-based water quality index. *Water Res.* **2020**, *179*, 115867. [[CrossRef](#)]
24. Kaur, L.; Rishi, M.S.; Siddiqui, A.U. Deterministic and probabilistic health risk assessment techniques to evaluate non-carcinogenic human health risk (NHHR) due to fluoride and nitrate in groundwater of Panipat, Haryana, India. *Environ. Pollut.* **2020**, *259*, 113711. [[CrossRef](#)] [[PubMed](#)]
25. Zhang, Q.; Qian, H.; Xu, P.; Hou, K.; Yang, F. Groundwater quality assessment using a new integrated-weight water quality index (IWQI) and driver analysis in the Jiakou Irrigation District, China. *Ecotoxicol. Environ. Saf.* **2021**, *212*, 111992. [[CrossRef](#)] [[PubMed](#)]
26. Mohanta, V.L.; Singh, S.; Mishra, B.K. Human health risk assessment of fluoride-rich groundwater using fuzzy-analytical process over the conventional technique. *Groundw. Sustain. Dev.* **2020**, *10*, 100291. [[CrossRef](#)]
27. Wang, Y.; Li, P. Appraisal of shallow groundwater quality with human health risk assessment in different seasons in rural areas of the Guanzhong Plain (China). *Environ. Res.* **2022**, *207*, 112210. [[CrossRef](#)]
28. Qasemi, M.; Darvishian, M.; Nadimi, H.; Gholamzadeh, M.; Afsharnia, M.; Farhang, M.; Allahdadi, M.; Darvishian, M.; Zarei, A. Characteristics, water quality index and human health risk from nitrate and fluoride in Kakhk city and its rural areas, Iran. *J. Food Compos. Anal.* **2023**, *115*, 104870. [[CrossRef](#)]
29. APHA. *Standard Methods for the Examination of Water and Wastewater*, 21st ed.; American Public Health Association/American Water Works Association/Water Environment Federation: Washington, DC, USA, 2005.
30. Deutsch, W.J. *Groundwater Geochemistry Fundamentals and Application to Contamination*; Lewis Publishers: Boca Raton, FL, USA, 1997.
31. Kant, N.; Singh, P.K.; Kumar, B. Hydrogeochemical characterization and groundwater quality of Jamshedpur urban agglomeration in Precambrian Terrain, Eastern India. *J. Geol. Soc. India* **2018**, *92*, 67–75. [[CrossRef](#)]
32. Jiang, Y.; Wu, Y.; Yuan, D. Human impacts on karst groundwater contamination deduced by coupled nitrogen with strontium isotopes in the Nandong Underground River System in Yunan, China. *Environ. Sci. Technol.* **2019**, *15*, 7676–7683. [[CrossRef](#)]
33. U.S. Environmental Protection Agency. *A Risk Assessment Multi-Way Exposure Spreadsheet Calculation Tool*; United States Environmental Protection Agency: Washington, DC, USA, 2014.
34. Kaiser, H.F. The application of electronic computers to factor analysis. *Educ. Psychol. Meas.* **1960**, *20*, 141–151. [[CrossRef](#)]
35. Barzegar, R.; Asghari Moghaddam, A.; Tziritis, E.; Fakhri, M.S.; Soltani, S. Identification of hydrogeochemical processes and pollution sources of groundwater resources in the Marand plain, northwest of Iran. *Environ. Earth Sci.* **2017**, *76*, 297. [[CrossRef](#)]
36. Elisante, E.; Muzuka, A.N.N. Assessment of sources and transformation of nitrate in groundwater on the slopes of Mount Meru, Tanzania. *Environ. Earth Sci.* **2016**, *75*, 277. [[CrossRef](#)]
37. Luo, Y.; Xiao, Y.; Hao, Q.; Zhang, Y.; Zhao, Z.; Wang, S.; Dong, G. Groundwater geochemical signatures and implication for sustainable development in a typical endorheic watershed on Tibetan plateau. *Environ. Sci. Pollut. Res.* **2021**, *28*, 48312–48329. [[CrossRef](#)] [[PubMed](#)]
38. World Health Organization. *Guidance for Immunotoxicity Risk Assessment for Chemicals*; IPCS Harmonization Project Document No. 10; World Health Organization: Geneva, Switzerland, 2011.
39. Yuan, L.; Fei, W.; Jia, F.; Jun-pong, L.; Qi, L.; Fang-ru, N.; Xu-dong, L.; Shu-lian, X. Health risk in children to fluoride exposure in a typical endemic fluorosis area on Loess Plateau, north China, in the last decade. *Chemosphere* **2020**, *243*, 125451. [[CrossRef](#)] [[PubMed](#)]

40. Mohammadi, A.A.; Yousefi, M.; Yaseri, M.; Jalilzadeh, M.; Mahvi, A.H. Skeletal fluorosis in relation to drinking water in rural areas of West Azerbaijan, Iran. *Sci. Rep.* **2017**, *7*, 17300. [CrossRef] [PubMed]
41. Gizaw, B. The origin of high bicarbonate and Fluoride concentration in waters of the Main Ethiopian Rift Valley, East African Rift system. *J. Afr. Earth Sci.* **1996**, *22*, 391–402. [CrossRef]
42. Banks, D.; Reimann, C.; Røyset, O.; Skarphagen, H.; Sæther, O.M. Natural concentrations of major and trace elements in some Norwegian bedrock groundwaters. *Appl. Geochem.* **1995**, *10*, 1–16. [CrossRef]
43. Adimalla, N.; Li, P. Occurrence, health risks, and geochemical mechanisms of Fluoride and nitrate in groundwater of the rock-dominant semi-arid region, Telangana State, India. *Hum. Ecol. Risk Assess. Int. J.* **2019**, *25*, 81–103. [CrossRef]
44. WHO. *Guidelines for Drinking-Water Quality*, 4th ed.; Incorporating First Addendum; World Health Organization: Geneva, Switzerland, 2017. Available online: <https://www.who.int/publications/i/item/9789241549950> (accessed on 14 January 2021).
45. Karunanidhi, D.; Subramani, T.; Roy, P.D.; Li, H. Impact of groundwater contamination on human health. *Geochem. Health* **2021**, *43*, 643–647. [CrossRef]
46. Khan, R.; Jhariya, D.C. Groundwater quality assessment for drinking purpose in Raipur city, Chhattisgarh using water quality index and geographic information system. *J. Geol. Soc. India* **2017**, *90*, 69–76. [CrossRef]
47. Jafari, S.M.; Nikoo, M.R. Developing a fuzzy optimization model for groundwater risk assessment based on improved DRASTIC method. *Environ. Earth Sci.* **2019**, *78*, 109. [CrossRef]
48. Jafari, S.M.; Nikoo, M.R. Groundwater risk assessment based on optimization framework using DRASTIC method. *Arab. J. Geosci.* **2016**, *9*, 742. [CrossRef]
49. Jafari, A.; Kamarehie, B.; Ghaderpoori, M.; Khoshnamvand, N.; Birjandi, M. The concentration data of heavy metals in Iranian grown and imported rice and human health hazard assessment. *Data Brief.* **2018**, *16*, 453–459. [CrossRef]
50. Aravinthasamy, P.; Karunanidhi, D.; Subramani, T.; Srinivasamoorthy, K.; Anand, B. Geochemical evaluation of Fluoride contamination in groundwater from Shanmuganadhi River basin, South India: Implication on human health. *Environ. Geochem. Health* **2019**, *42*, 1937–1963. [CrossRef]
51. He, S.; Wu, J. Relationships of groundwater quality and associated health risks with land use/land cover patterns: A case study in a loess area, Northwest China. *Hum. Ecol. Risk Assess.* **2019**, *25*, 354–373. [CrossRef]
52. Ahada, C.P.S.; Suthar, S. Assessment of Human Health Risk Associated with High Groundwater Fluoride Intake in Southern Districts of Punjab, India. *Expo. Health* **2019**, *11*, 267–275. [CrossRef]
53. Karunanidhi, D.; Aravinthasamy, P.; Subramani, T.; Roy, P.D.; Srinivasamoorthy, K. Risk of Fluoride-rich groundwater on human health: Remediation through managed aquifer recharge in a hard rock terrain, South India. *Nat. Resour. Res.* **2019**, *29*, 2369–2395. [CrossRef]
54. Esteban, J.; Starr, A.; Willetts, R.; Hannah, P.; Bryanston, P. A Review of data fusion models and architectures: Towards engineering guidelines. *Neural Comput. Appl.* **2005**, *14*, 273–281. [CrossRef]
55. Huang, Z.-H.; Li, W.-J.; Wang, J.; Zhang, T. Face recognition based on pixel-level and feature-level fusion of the top-level's wavelet sub-bands. *Inf. Fusion* **2015**, *22*, 95–104. [CrossRef]
56. AbdelGawad, A.M.; Bayoumi, M.A. Remote Measuring for Sand in Pipelines Using Wireless Sensor Network. *IEEE Trans. Instrum. Meas.* **2011**, *60*, 1443–1452. [CrossRef]
57. Pandey, V.; Giri, V.K. High frequency noise removal from ECG using moving average filters. In Proceedings of the 2016 International Conference on Emerging Trends in Electrical Electronics & Sustainable Energy Systems (ICETEESES), Sultanpur, India, 11–12 March 2016. [CrossRef]
58. Carrillo-Rivera, J.J.; Cardona, A.; Edmunds, W.M. Use of abstraction regime and knowledge of hydrogeological conditions to control high-fluoride concentration in abstracted groundwater: San Luis Potosí basin, Mexico. *J. Hydrol.* **2002**, *261*, 24–47. [CrossRef]
59. Hounslow, A. *Water Quality Data: Analysis and Interpretation*; CRC Publication LLD.: Boca Raton, FL, USA, 1995; p. 381.
60. Asghari Moghaddam, A.; Fijani, E. Distribution of fluoride in groundwater of Maku area, northwest of Iran. *Environ. Geol.* **2008**, *56*, 281–287. [CrossRef]
61. Tekle-Haimanot, R.; Melaku, Z.; Kloos, H.; Reimann, C.; Fantaye, W.; Zerihun, L.; Bjorvatn, K. The geographic distribution of fluoride in surface and groundwater in Ethiopia with an emphasis on the Rift Valley. *Sci. Total Environ.* **2006**, *367*, 182–190. [CrossRef] [PubMed]
62. Gopinath, S.; Srinivasamoorthy, K.; Saravanan, K.; Suma, C.S.; Prakash, R.; Senthinathan, D.; Sarma, V.S. Vertical electrical sounding for mapping saline water intrusion in coastal aquifers of Nagapattinam and Karaikal, South India. *Sustain. Water Resour. Manag.* **2018**, *4*, 833–841. [CrossRef]
63. Sarma, D.R.R.; Rao, S.L.N. Fluoride concentrations in groundwaters of Visakhapatnam, India. *J. Environ. Contam. Toxicol.* **1997**, *58*, 241–247.
64. Egbueri, J.C.; Mgbenu, C.N.; Chukwu, C.N. Investigating the hydrogeochemical processes and quality of water resources in Ojoto and environs using integrated classical methods. *Model. Earth Syst. Environ.* **2019**, *5*, 1443–1461. [CrossRef]
65. Mgbenu, C.N.; Egbueri, J.C. The hydrogeochemical signatures, quality indices and health risk assessment of water resources in Umunya district, southeast Nigeria. *Appl. Water Sci.* **2019**, *9*, 1–19. [CrossRef]
66. Anawar, H.M.; Akai, J.; Komaki, K.; Terao, H.; Yoshioka, T.; Ishizuka, T.; Safiullah, S.; Kato, K. Geochemical occurrence of arsenic in groundwater of Bangladesh: Sources and mobilization processes. *J. Geochem. Explor.* **2003**, *77*, 109–131. [CrossRef]

67. Levins, I.; Gosk, E. Trace elements in groundwater as indicators of anthropogenic impact. *Environ. Geol.* **2008**, *55*, 285–290. [[CrossRef](#)]
68. Tomar, V.; Prasad, S.; Kumar, D. Adsorptive removal of fluoride from aqueous media using *Citrus limonum* (lemon) leaf. *Microchem. J.* **2014**, *112*, 97–103. [[CrossRef](#)]
69. Yadav, A.K.; Abbassi, R.; Gupta, A.; Dadashzadeh, M. Removal of fluoride from aqueous solution and groundwater by wheat straw, sawdust and activated bagasse carbon of sugarcane. *Ecol. Eng.* **2013**, *52*, 211–218. [[CrossRef](#)]
70. Yadav, K.K.; Singh, J.K.; Gupta, N.; Kumar, V. A review of nanobioremediation technologies for environmental cleanup: A novel biological approach. *J. Mater. Environ. Sci.* **2017**, *8*, 740–757.
71. Jorfi, S.; Rezaei Kalantary, R.; Mohseni Bandpi, A.; Jaafarzadeh Haghighifard, N.; Esrafil, A.; Alaei, L. Fluoride removal from water by adsorption using bagasse, modified bagasse and chitosan. *Iran. J. Health Environ.* **2011**, *4*, 35–48.
72. Asgari, G.; Roshani, B.; Ghanizadeh, G. The investigation of kinetic and isotherm of fluoride adsorption onto functionalize pumice stone. *J. Hazard Mater.* **2012**, *217*, 123–132. [[CrossRef](#)] [[PubMed](#)]
73. Rahmani, A.; Nouri, J.; Ghadiri, S.K.; Mahvi, A.H.; ZareM, R. Adsorption of fluoride from water by Al³⁺ and Fe³⁺ pretreated natural Iranian zeolites. *Int. J. Environ. Res.* **2010**, *4*, 607–614.
74. Khatibikamal, V.; Torabian, A.; Janpoor, F.; Hoshyaripour, G. Fluoride removal from industrial wastewater using electrocoagulation and its adsorption kinetics. *J. Hazard Mater.* **2010**, *179*, 276–280. [[CrossRef](#)]
75. Malakootian, M.; Yousefi, N.; Fatehizadeh, A. Survey efficiency of electrocoagulation on nitrate removal from aqueous solution. *Int. J. Environ. Sci. Technol.* **2011**, *8*, 107–114. [[CrossRef](#)]
76. Behbahani, M.; Moghaddam, M.A.; Arami, M. Techno-economical evaluation of fluoride removal by electrocoagulation process: Optimization through response surface methodology. *Desalination* **2011**, *271*, 209–218. [[CrossRef](#)]
77. Emamjomeh, M.M.; Sivakumar, M. An empirical model for defluoridation by batch monopolar electrocoagulation/flotation (ECF) process. *J. Hazard Mater.* **2006**, *131*, 118–125. [[CrossRef](#)]
78. Bazrafshan, E.; Ownagh, K.A.; Mahv, A.H. Application of electrocoagulation process using iron and aluminum electrodes for fluoride removal from aqueous environment. *J. Chem.* **2012**, *9*, 2297–2308. [[CrossRef](#)]
79. Poursaberi, T.; Hassanisadi, M.; Torkestani, K.; Zare, M. Development of zirconium (IV)-metalloporphyrin grafted Fe₃O₄ nanoparticles for efficient fluoride removal. *Chem. Eng. J.* **2012**, *189*, 117–125. [[CrossRef](#)]
80. Hosseini, M.; Fazelian, N.; Fakhri, A.; Kamyab, H.; Yadav, K.K.; Chelliapan, S. Preparation, and structural of new NiS-SiO₂ and Cr₂S₃-TiO₂ nano-catalyst: Photocatalytic and antimicrobial studies. *J. Photochem. Photobiol. B* **2019**, *194*, 128–134. [[CrossRef](#)] [[PubMed](#)]
81. Samatya, S.; Yüksel, Ü.; Yüksel, M.; Kabay, N. Removal of fluoride from water by metal ions (Al³⁺, La³⁺ and ZrO²⁺) loaded natural zeolite. *Separ. Sci. Technol.* **2007**, *42*, 2033–2047. [[CrossRef](#)]
82. National Academy of Sciences (NAS). *Science and Decisions: Advancing Risk Assessment*; National Academy Press: Washington, DC, USA, 2009.
83. Sedghi, Z.; Rostami, A.A.; Khatibi, R.; Nadiri, A.A.; Sadeghfam, S.; Abdoallahi, A. Chapter 11—Mapping and aggregating groundwater quality indices for aquifer management using Inclusive Multiple Modeling practices. In *Risk, Reliability and Sustainable Remediation in the Field of Civil and Environmental Engineering*; Elsevier: Amsterdam, The Netherlands, 2022; pp. 155–182. [[CrossRef](#)]
84. Huang, J.; Ling, C. Using AUC and accuracy in evaluating learning algorithms. *IEEE Trans. Knowl. Data Eng.* **2005**, *17*, 299–310. [[CrossRef](#)]
85. ASTEE (Association Scientifique et Technique de l’Eau et de l’Environnement). Guide Pour L’évaluation du Risque Sanitaire Dans le Cadre de L’étude D’impact D’une UIOM, 2003; 60p. Available online: <https://temis.documentation.developpement-durable.gouv.fr/docs/Temis/0070/Temis-0070209/18437.pdf> (accessed on 30 September 2022).